ON THE DESIGN OF FLUXONICS: REVERSIBLE SUPERCONDUCTING CIRCUITS

by

Dewan Jermaine Woods

A Dissertation

Submitted to the Faculty of Purdue University

In Partial Fulfillment of the Requirements for the degree of

Doctor of Philosophy

Department of Physics and Astronomy

West Lafayette, Indiana

August 2022

THE PURDUE UNIVERSITY GRADUATE SCHOOL
STATEMENT OF COMMITTEE APPROVAL

Dr. Rudro R. Biswas, Chair

Department of Physics and Astronomy

Dr. Erica Carlson

Department of Physics and Astronomy

Dr. Srividya Iyer-Biswas

Department of Physics and Astronomy

Dr. Birgit Kaufmann

Department of Physics and Astronomy

Approved by:

Dr. Gabor Csathy

To the entire Woods family

ACKNOWLEDGMENTS

I have always had a healthy curiosity about the sciences, and oftentimes, was annoyingly inquisitive as a child. I recall completely taking a part my mother's brand new 5-disc CD player at age 9 – while it was fun and satisfying at the time, it did not end well for me when she found out about what I had done. The moment I entered my first physics course in high school, I knew that I had found the branch of science that I wanted to dedicate my life to. I even hung up my gloves and gave up boxing for physics. Seeing the equations on the board predict and accurately depict the nature of the result of small experimental set-ups was the closest thing to magic that I had ever seen. Fast forward to today, I've witnessed lots more, learned lots more, and met incredible people along the way, whom I am grateful for and whom I wish to take the opportunity to thank.

I thank my mother and the entire Woods family. As the first in my family to go to college, they have all been my biggest supporters, especially my mother – one of the funniest people I know. She supports me in all that I do. I also thank my grandparents, my uncles, younger brother, and cousins for all their words of encourage, despite not having much of a clue of what I do, but knowing that I was doing what I loved to do.

I have always maintained that year 2006 was one of the most important years of my life. 101 years after Albert Einstein had his "miracle year", perhaps I had my own, in terms of meeting someone who motivated me more than ever. It was my first year of high school when I entered the classroom of Dr. Erinn Wilcots. No one ever pushed me harder to succeed and I am forever grateful to have her in my life.

I thank my closest friend, Cortney. A week after starting my PhD, I literally bumped into her, knocking her over onto the ground. I felt terrible at that moment, helped her up, and we've been the best of friends ever since then. She's thrown me an amazing birthday party every year of my graduate school career. Thank you for all the years of laughter, all the enlightening and philosophical conversations, and friendly debates. It was a great pleasure and escape talking and making music with you. I look forward to more great moments in the future.

I thank my very close friend, Dr. Virginia Soldino for all the great moments we shared traveling, all the great conversations, and for all the inspiration. I also thank her for all the amazing Spanish food she's cooked for me over the years.

I thank Prof. Gabor Csathy for all of his advice and words of encourage. We'd often greet one another in the department and met officially at the March meeting in Boston, where we had a conversation about research and science in general.

I thank Prof. Sherwin Love for all of his helpful advice.

I would like to thank, Prof. Srividya Iyer-Biswas, Prof. Birgit Kaufmann, and Prof. Erica Carlson for agreeing to be on my committee. Also, special thanks to Prof. Carlson for the great advice, conversations, and words of encourage over the years. She was the very first Purdue Physics faculty I met and spoke with upon my arrival.

I thank my advisor, Prof. Rudro R. Biswas, for agreeing to take me on as a student. I learned a lot over the years, including newer ways to go about thinking about things, which took some time and conditioning to adjust my mind to visualize certain aspects of physics in certain ways that I had not thought about or perceived before. Prof. Biswas is extremely gifted, scientifically and mathematically, and is the epitome of a true scientist, in striving to understanding anything and everything about a scientific problem, all the way down to the root.

I especially thank him for involving me on the project with Sandia National Lab experimental collaborators, which turned into my dissertation project. I also thank him for his extensive help in seeing this dissertation through to finish. In this context, special thanks also to Rishabh Khare, another group member in Prof. Biswas's group, who has contributed substantial portions of the collaborative project we synergistically worked on.

I thank my colleagues and office mates, Guodong, Yingkang, in addition to Rishabh. Special thank you to Sandy and Janice for all their help over the years.

TABLE OF CONTENTS

LIST OF TABLES

LIST OF FIGURES

ABSTRACT

In this dissertation, we present work on developing superconducting circuits intended to advance the implementation of Asynchronous Ballistic Reversible Computation using Fluxon Logic. In the first Chapter we introduce the need for developing reversible computing, and discuss implementing asynchronous reversible computing using fluxons in superconducting circuits. In Chapter 2, we introduce basic superconductivity physics, including the Josephson effects, which is necessary to know for understanding the behavior of Josephson junction transmission lines. In Chapter 3, we introduce tools to physically understand the behavior of topologically protected solitons, 'fluxons', in Josephson junction transmission lines. Finally, in Chapter 4, we briefly discuss the history of fluxon-based computation devices and present current state of the art design of such reversible computation devices, including the fluxon Rotary gate that we have developed. Taken together, these represent advances in the direction of implementing asynchronous reversible computing in practice.

1. OVERVIEW, BACKGROUND, AND MOTIVATION

The overarching motivation for my work presented in this dissertation is to formulate the basic theoretical rules governing reversible superconducting circuits. Achieving this outcome entails reaching the following goals: (a) developing a theory of asynchronous ballistic reversible logic (ABRL) gates, (b) constructing realistic model of Josephson junction (JJ) circuits that implement such reversible logic gates and (c) quantifying the origin of energy losses in the system so that these losses can ultimately be reduced with appropriate design choices. My original contributions are mainly in goal (b); goal (a) has been under development by my collaborators at Sandia National Laboratory while achieving goal (c) lies in the future. I will, however, give brief discussions of progress along both goals (a) and (c), which will also provide adequate context for discussing my contributions to goal (b).

Computers are involved in more and more aspects of today's society - entertainment, communication, information storage, security, etc. Naturally, computational power and energy efficiency associated with today's computers are the focus of much attention. Progress in computational performance relative to power consumed is gradually stalling as we near the end of Moore's Law. This has prompted a broad quest for finding new breakthroughs in computing performance. Asynchronous Reversible Ballistic Computing (ABRC) [1] is a paradigm suggested for achieving this quest by reducing energy consumption below the Landauer limit (see below). In this dissertation, I will consider superconducting circuits that use ballistic fluxon propagation to implement this computation paradigm. Figure (1.1) shows the trend of the 10 best known supercomputers. China's Sunway Tianhu Light is the most powerful computer in the world, performing 93 petaflops/sec while consuming about 16 megawatts of power. High performance computing in conventional complementary metal-oxide-semiconductor (CMOS) technology uses lots of energy and if we want to see the continued growth and progressing trend in supercomputer performance, the exploration of new approaches is essential. How can we progress to higher levels of performance for lower power?

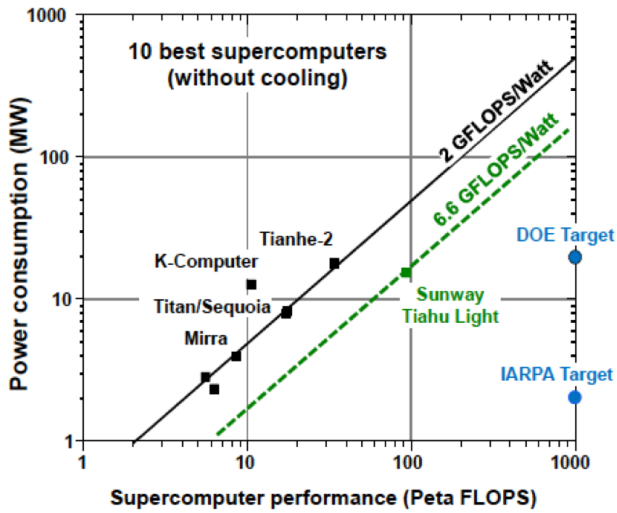

Figure 1.1. Trend high performance supercomputers power consumption for the 10 best supercomputers. (Image credit: Mark A. Gouker, MIT Lincoln Lab)

1.1 Landauer's Principle and Reversible Computation

Any computation requires energy and how much energy we use is an issue of great concern. Rolf Landauer, in 1961, formulated a statement, now known as the Landauer principle, which states that dissipative, irreversible computation (all computers currently work like this) requires at least $k_B T \ln 2$ energy per bit operation, where k_B is Boltzmann's constant and T the operating temperature. This is a theoretical limit of consumption of computational power - any logically irreversible manipulation of a bit of information, exemplified by the resetting of a bit in a memory register, will generate an entropy increase of at least $k_B \ln 2$. See Figure 1.2 for how the Landauer limit compares with the landscape of energy usage by various computational platforms.

Reversible computation is a computational paradim for avoiding the Landauer limit by involving only reversible bit operations. The concept of reversible computation has a storied history[2], with the first theoretical prototype of a logic gate being proposed by Edward Fredkin and Tommaso Toffoli[3]. In such a computational paradigm, one can configures logic gates to redirect inputs conditionally towards unique outputs [4], thereby conserving

entropy. Computer scientists argue that if one could thus transform states in a one-to-

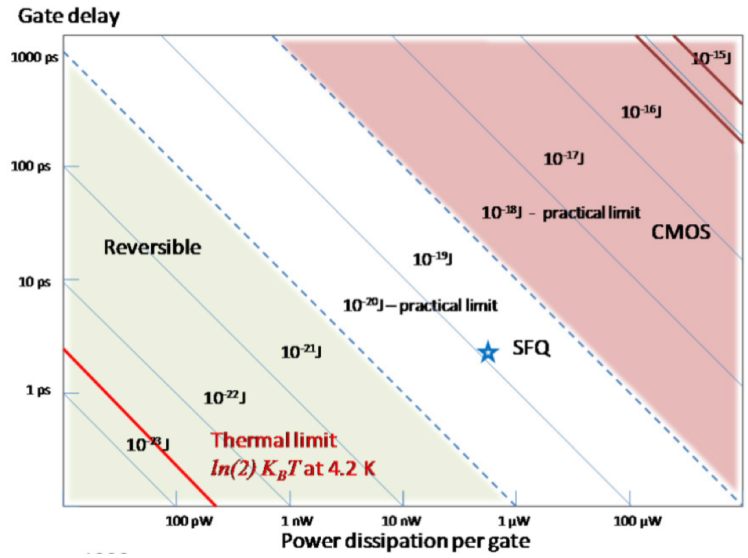

Figure 1.2. Gate delay time vs the power dissipation per gate for distinctive computing systems. (Image credit: [5])

one fashion, no information will be destroyed and entropy would not be generated - the computer could theoretically operate with gates dissipating less than $k_B T \ln 2$ of energy per operation. Gates approaching zero energy dissipation could additionally be run in reverse and with no minimum energy dissipation; there is no reduction in information in a closed cycle [4] that ends with the system in the same initial state, and hence no Landauer-type dissipation. Shown in fig. 1.2 is the relationship between gate delay time and the associated power dissipation per gate, as developed by the computer science community. There is an obvious distinction between reversible and irreversible (CMOS) approaches to computing - the reversible approach offers shorter gate delay times for much lower power consumption. If we wish to compute at energies below the thermal limit, reversible systems must be employed.

1.2 Asynchronous Ballistic form of Reversible Logic (ABRL)

Original formulations of reversible computing required unrealistic conditions like precise clock control of the arrival times of bits at logic gates. Asynchronous ballistic reversible computation (ABRC) [1], a type of reversible computation that can perform universal logic

operations, is a modern prescription for avoiding such drawbacks by allowing different bits to arrive at logic gates asynchronously.

Fig. 1.3 shows a schematic that draws the clear distinction between both synchronous and asynchronous ballistic configurations. Synchronous ballistic configuration, requiring precise timing, has proved to be too impractical to achieve. Such timing uncertainties are also amplified chaotically when signals interact in larger synchronous circuits (a form of entropy increase). The asynchronous configuration allows for much looser timing constraints and has a linear increase in timing uncertainty per logic state as opposed to an exponential increase for the synchronous configuration. ABRC also significantly simplifies circuit design as the need for clocking networks is reduced. ABRC thus provides a more realistic paradigm for implementing energy-efficient reversible computation. Constructing ABRC logic gates implemented using superconducting fluxons is the main goal of this dissertation, with the long term goal of constructing realistic highly energy-efficient computers.

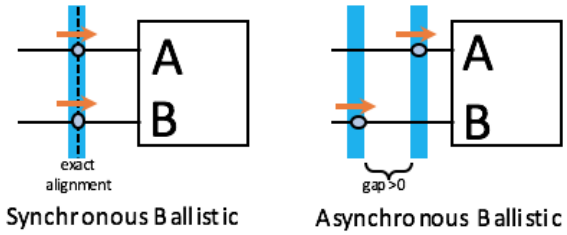

Figure 1.3. Schematic of both synchronous and asynchronous ballistic configuration. (Image credit: Dr. Rupert Lewis, Sandia NL.)

1.3 Asynchronous Ballistic Reversible Fluxon Logic using Superconducting Circuits

Asynchronous ballistic reversible logic requires technology that is inherently low loss and dissipationless superconducting elements are perfectly suitable for this idea[6]. Specifically, superconducting circuits operating in the reversible regime with single flux quanta (fluxons) being used to encode data have been demonstrated to be highly energy-efficient, with out-

put fluxons retaining up to 97% of their input energy [7] (compare with resistive nature of transistor-based circuits). As detailed below, such fluxon logic circuits are built using superconducting Josephson junction (JJ) switches and superconducting interconnects. Logic in such superconducting circuits is based on the presence or absence of a magnetic flux quantum (fluxons) trapped in a superconducting wire loop – fluxons are topologically quantized stable objects that can exhibit ballistic propagation at low temperatures since they are solitonic excitations in these circuits[6], [8]. Ballistically propagating bits, a basic requirement for constructing ABRC, can then be encoded as single flux quanta (SFQ).

The long term goal of the research presented in this dissertation is this: to design implementable low-dissipation ABRC fluxon logic structures in realistic superconducting networks composed of superconducting wires (inductance elements) and Josephson junctions (weak links/switches).

2. SUPERCONDUCTIVITY AND THE JOSEPHSON EFFECTS

2.1 Introduction

Superconductors are substances (superconductors) which, upon cooling below a characteristic critical temperature, exhibit zero DC electrical resistance which also expel magnetic fields from the bulk. Both these characteristics constitute a hallmark of the property of superconductivity.

When cooling a (metallic) conductor at room temperaturs, the resistance decreases gradually. Kamerlingh Onnes, curious about the low resistance behavior of metals when cooled to near absolute zero temperatures and having also liquefied Helium (Nobel prize, 1913) that enabled him to achieve that end, conducted an experiment seeking insight to the temperature dependence of the resistivity of Mercury [9]. He found that at $T = 4.20K$, there existed

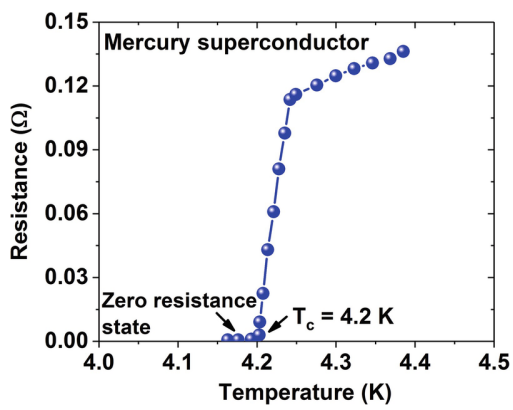

Figure 2.1. Onnes' experimental result for the temperature dependence of the resistivity of Mercury [9], reproduced from [10].

a sharp transition as Mercury's resistivity abruptly vanished to levels below detection limits. In this way, superconductivity was discovered in 1911.

Decades of research followed, some selected highlights being discovery of the Meissner effect [11] (1933), i.e., the characteristic magnetic flux expulsion from superconductors that distinguish them from just 'very good conductors'; the Landau-Ginzburg effective theory of superconductivity [12] (Nobel prizes, 1962 and 2003[13]); and the quantum mechanical microscopic Bardeen-Cooper-Schrieffer theory of superconductivity[14] (Nobel prize, 1972).

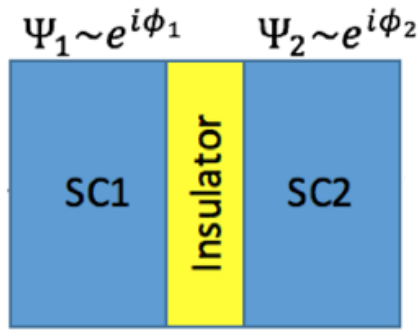

Figure 2.2. Schematic of a Josephson junction, consisting of an insulating material sandwiched by two superconductors of different order parameters.

Finally, in 1962, Brian Josephson considered seriously a novel element of the Landau-Ginzburg theory – the concept of a complex superconducting order parameter whose gradient is related to the supercurrent – and proposed that a supercurrent can flow without any voltage drop between two superconducting electrodes that are separated by a thin barrier [15] (Nobel prize, 1973). Such a junction, a 'Josephson' junction, can support a current up to a characteristic critical current, I_c, before deviating into the resistive, dissipative regime (see Figure 2.3). This supercurrent is given by the Josephson relation [16]

$$I_s = I_c \sin \phi \tag{2.1}$$

where $\phi = \phi_2 - \phi_1$ is the difference between phases of the complex Ginzburg-Landau order parameters of the two superconducting electrodes. This is the DC Josephson effect. Moreover, if a constant voltage is maintained across the junction, the phase difference evolves according to [17]

$$\frac{d\phi}{dt} = \frac{2\mathrm{e}V}{\hbar}. \tag{2.2}$$

Using equation (2.1), we see that a steadily changing ϕ giving rise to an alternating current of frequency $2\mathrm{e}V/h$ [18]; thus, the Josephson junction can be used to relate frequency to voltage with a universal conversion factor composed of material-agnostic fundamental con-

stants! This is the AC Josephson effect and has been used for defining the Josephson voltage standard.

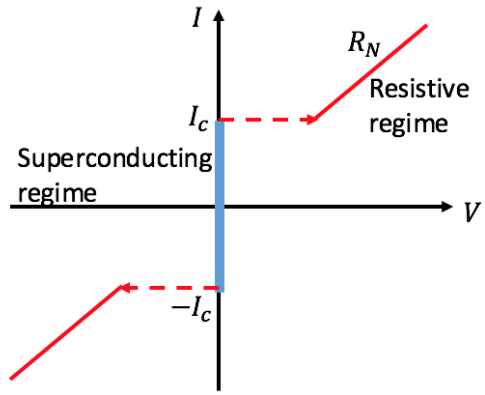

Figure 2.3. Typical I-V curve for a Josephson junction.

Fig. 2.3 shows a typical IV curve of a JJ - as the system is biased up to the critical current, I_c, the system remains in its superconductor state. When the applied current exceeds I_c, the system transitions to its dissipative state.

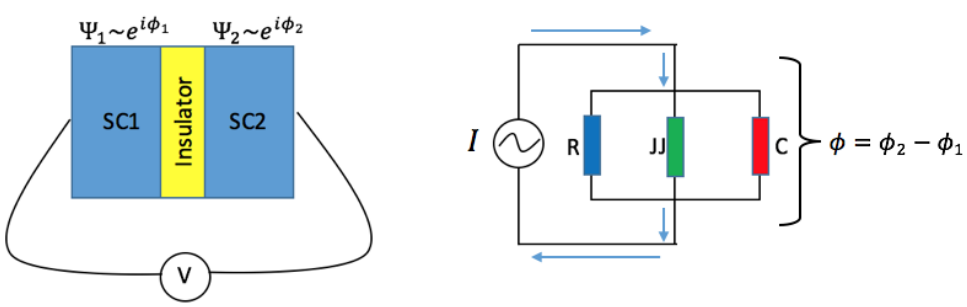

Figure 2.4. A real Josephson junction (left) is composed of an insulating barrier sandwiched between two superconductors, the phases, $\phi_{1,2}$, of whose order parameters, $\Psi_{1,2}$ respectively, differ by an amount ϕ. It is well-modeled by the RCSJ model (right) consisting of a shunt resistor, a shunt capacitor and an ideal Josephson junction connected in parallel.

2.2 The Resistively and Capacitively Shunted Junction (RCSJ) model

While equation (2.1) suffices to describe zero voltage (stationary) properties of Josephson junctions, situations involving non-zero, finite voltages need a more extensive description. Realistic JJs have been found to be adequately described by the resistively and capacitively shunted junction (RCSJ) model [17]. Fig. 2.4 shows a schematic layout of the RCSJ circuit model of a real Josephson junction, consisting of a shunt resistor (due to conductance arising from, say, thermally excited quasiparticles), a shunt capacitor (due to interfacial charges at the contacts with superconducting leads) and an ideal Josephson junction connected in parallel.

I will now use this model to describe the dynamics of a realistic JJ. Consider the dynamics of the simple circuit shown in Figure 2.4. The total current flowing through the system is given by

$$I = I_{jj} + I_{res} + I_{cap}, \tag{2.3}$$

the three currents on the RHS being those passing through the ideal JJ, the shunt resistor and the shunt capacitance, respectively. Replacing by respective behaviors,

$$I = I_c \sin\phi + \frac{V}{R} + C\frac{dV}{dt}, \tag{2.4}$$

wherein ϕ is the phase difference across the ideal JJ, I_c its critical current, V the voltage across the JJ, R the value of the shunt resistance and C the value of the shunt capacitace. Incorporating equation (2.2), we obtain the current solely as a function of the phase difference across the JJ:

$$I = I_c \sin\phi + \frac{\hbar}{2\mathrm{e}R}\frac{d\phi}{dt} + \frac{\hbar C}{2\mathrm{e}}\frac{d^2\phi}{dt^2}. \tag{2.5}$$

For drawing an analogy with classical mechanical systems, we can rewrite the above equation in the form:

$$\left(\frac{\hbar}{2\mathrm{e}}\right)^2 C\frac{d^2\phi}{dt^2} + \left(\frac{\hbar}{2\mathrm{e}}\right)^2 \frac{1}{R}\frac{d\phi}{dt} + \frac{d}{d\phi}\left[E_J\left(1 - \cos\phi - \frac{I}{I_c}\phi\right)\right] = 0 \tag{2.6}$$

where $E_J = \frac{\hbar I_c}{2e}$. Remarkably, as can be made clear by a cosmetic substitution $\phi(t) \to x(t)$, the reader can see that this is the differential equation governing the damped motion of a one-dimensional Newtonian particle in a tilted washboard potential whose tilting is controlled by the applied current (see also Figure 2.5):

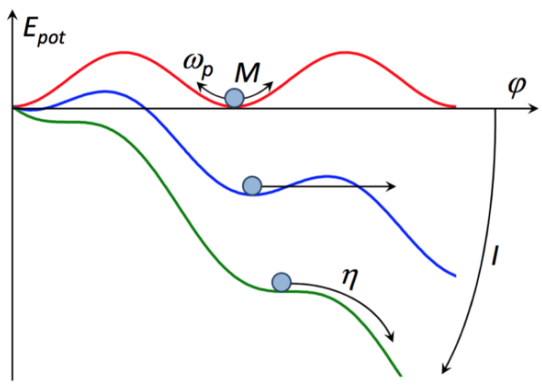

Figure 2.5. The motion of the phase across a JJ can be understood in analogy with the damped motion of a particle in the tilted washboard potential above (equations (2.6) and (2.7) in the main text). The instantaneous tilting of the potential is proportional to the instantaneous value of the current through the JJ. The tilting is enough to allow a particle to 'roll' on to the next well only when the applied current is greater than the critical current of the JJ. (Image credit: [19].)

$$M\frac{d^2x}{dt^2} + \eta\frac{dx}{dt} + \partial_x U(x) = 0, \tag{2.7}$$

where the mass is $M = (\hbar/(2e))^2 C$, the friction coefficient is $\eta = (\hbar/(2e))^2/R$, and the tilted washboard potential is given by $U(x) = E_J(1 - \cos x - (I/I_c)x)$.

2.3 Response to External Current Source

To gain insight into the driven dynamics of Josephson junctions, I will now consider a realistic junction, described by the RCSJ model as in Figure 2.4, being driven by an external

current source. In particular, I will consider a sinusoidal current source, $I(t) = I_0 \sin \omega t$, oscillating at angular frequency ω. Substituting in equation (2.5):

$$I_0 \sin \omega t = I_c \sin \phi + \frac{\hbar}{2\mathrm{e}R}\frac{d\phi}{dt} + \frac{\hbar C}{2\mathrm{e}}\frac{d^2\phi}{dt^2}. \tag{2.8}$$

Rewriting this expression,

$$\frac{\hbar C}{2\mathrm{e}I_c}\frac{d^2\phi}{dt^2} + \frac{\hbar}{2\mathrm{e}RI_c}\frac{d\phi}{dt} + \left(\sin\phi - \alpha \sin \omega t\right) = 0 \tag{2.9}$$

where $\alpha = \frac{I_0}{I_c}$. Setting $\tau \equiv t/\tau_c$, where $\tau_c = \hbar/(2\mathrm{e}I_cR)$ is the 'Josephson time constant' – relaxation time constant for the particle to come to a halt in the washboard potential of Figure 2.5, we can rewrite the equation in a dimensionless form:

$$\frac{\hbar C}{2\mathrm{e}I_c\tau_c^2}\frac{d^2\phi}{d\tau^2} + \frac{\hbar}{2\mathrm{e}RI_c\tau_c}\frac{d\phi}{d\tau} + \left(\sin\phi - \alpha \sin \omega\tau_c\tau\right) = 0, \tag{2.10}$$

$$\Rightarrow \beta_c\frac{d^2\phi}{d\tau^2} + \frac{d\phi}{d\tau} + \left(\sin\phi - \alpha \sin \omega\tau_c\tau\right) = 0. \tag{2.11}$$

Herein, $\beta_c = 2\mathrm{e}I_cR^2C/\hbar$ is dimensionless parameter, known as the Stewart-McCumber parameter [20], [21]. β_c is also inversely related to the damping of the junction and is thus related to its quality factor, $Q = \sqrt{\beta_c}$. Typical values of various RCSJ parameters for Josephson junctions, used by my experimental collaborators for constructing fluxon networks, are listed in Table 2.1.

Table 2.1. Typical JJ parameters in JJ circuits.

Quantity	**Value**
β_c, $\frac{2\mathrm{e}I_cR^2C}{\hbar}$	0.5436
Frequency, ω	10^9Hz
Critical Current, I_c	100μA
Resistance, R	1.6 Ω
Capacitance, C	700fF
α, $\frac{I_0}{I_c}$	$\mathcal{O}(1)$

The formulation in equation 2.11, coupled with the physical picture shown in Figure 2.5, allows us to delineate characteristic limiting behaviors of the JJ, especially in the DC driven limit ($\omega\tau_c \ll 1$).

For $\beta_c \ll 1$, the 'overdamped' regime (the dissipative first derivative term is dominant over the intertial second derivative term), when driving current amplitude is below I_c, i.e., $\alpha < 1$, the junction quickly settles to a static value of the phase such that $\sin\phi = I(t)/I_c$. The final voltage drop is zero across the junction. This corresponds to a damped particle slowing to a stop within a single well in a quasi-static slightly tilted washboard potential in Figure 2.5. When the driving current rises above I_c, excess current has to be forced through the shunt resistor, resulting in oscillatory behavior of the superconducting phase. This corresponds to the particle in Figure 2.5 progressing down the washboard potential, tilted more than the critical steepness, with a velocity capped by a 'drift' value. When $\alpha \gg 1$, this is simply given by the Ohmic limit of $V = IR$, with a tiny oscillatory component on top due to the ideal JJ current $I_{JJ} = I_c \sin(2\mathrm{e}Vt/h)$. This is apparent from our intuition of a damped particle rolling down a very steep (compared to the corrugaton amplitude) washboard potential.

When the junction is 'underdamped', i.e., $\beta_c \gg 1$, the problem is equivalent to an undamped particle in the washboard potential of Figure 2.5. A new interesting phenomenon of hysteresis appears, which is exploited in certain JJ computational circuit designs (section 4.1). When the current is well above I_c, we have the same behavior as in the overdamped case, with $V = IR$. However, as the driving current is reduced to below I_c, i.e., the washboard potential in Figure 2.5 is slowly brought to level, the particle continues to move ahead with intertia, continuing to follow the Ohmic law $V = IR$ on the average. However, after a long enough time or if started from zero driving current to a value less than I_c, the particle settles into an equilibrium position in one well, settling to the usual Josephson current relation $\sin\phi = I(t)/I_c$, with zero voltage drop. In other words, an underdamped junction can be found in both 'resistive' or 'superconducting' regimes for $I < I_c$.

Further discussions can be accessed in standard textbooks [17]. Realistic JJs are usually somewhere in between, and I will study their dynamics by directly numerically solving equation (2.8).

2.4 The Meissner Effect - Magnetic Flux Quantization

Upon lowering the temperature of a metal to below its characteristic critical temperature, the metal will transition to its superconducting state. During this transition, the magnetic field is expelled from the superconductor - this is known as the Meissner effect and is a significant point of difference between a superconductor and a metal with negligible resistance[11]. This effect is behind the popular demonstration of magnets being levitated by superconductors.

There exists a simple relation between the phase of the superconducting order parameter and the magnetic flux through a non-superconducting region inside it (e.g., the hole inside a superconducting loop, or a superconducting vortex core). Inside the bulk superconductor at equilibrium, Landau-Ginzburg theory [12] says that the change of the complex order parameter phase is simply related to the line integral of the magnetic vector potential:

$$\phi(\vec{r}_2) - \phi(\vec{r}_1) = -\frac{2\mathrm{e}}{\hbar}\int_{\vec{r}_1}^{\vec{r}_2} d\vec{r}\cdot\vec{A}(\vec{r}). \tag{2.12}$$

If the path encloses a non-superconducting region 'NS', then using the fact that the superconducting phase, being the complex phase of a complex number field, can change by an integer multiple of 2π around a closed loop, we have using equation (2.12),

$$2m\pi = -\frac{2\mathrm{e}}{\hbar}\oint d\vec{r}\cdot\vec{A}(\vec{r}) = \frac{2\pi\Phi_B^{NS}}{\Phi_0}, \quad \text{i.e.,} \quad \Phi_B^{NS} = m\Phi_0, \tag{2.13}$$

wherein $\Phi_0 = h/(2\mathrm{e}) \simeq 2.068\times10^{-15}$ Wb is the universal superconducting flux quantum, Φ_B^{NS} is the magnetic flux through the enclosed non-superconducting region, and m is an integer. This is the famous equation of universal flux quantization showing that the magnetic flux through holes in the superconductor is quantized to be an integer multiple of the material-agnostic superconducting flux quantum[22], [23].

2.5 Phase Dynamics in JJ transmission lines

Interesting phenomena occur when a large number of discrete JJs are strung in parallel between superconducting lines, or equivalently, a long JJ (LJJ) is considered ('long' in the sense that the phase modulation can accommodate one fluxon well within the junction). Sketches of both possibilities are presented in Figure 2.6.

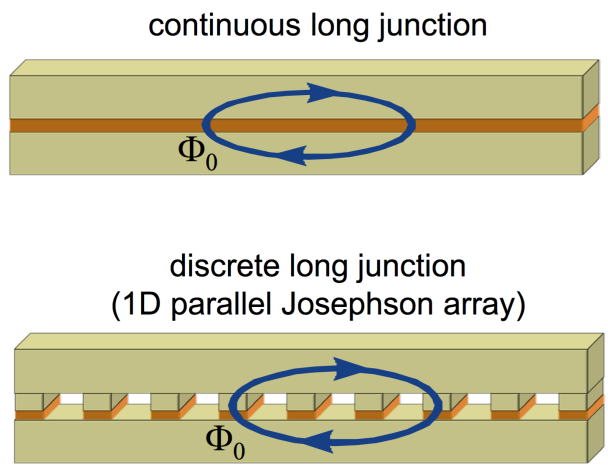

Figure 2.6. Schematic of both continuous and discrete long Josephson junction. (Image credit: [24].)

Figure 2.7 shows a circuit schematic corresponding to the discrete long junction. The region between two successive loops can enclose magnetic flux; this is modeled by the inductances on the top and bottom superconducting lines. We continue using the RCSJ model to describe the individual JJs, which we assume to be identical.

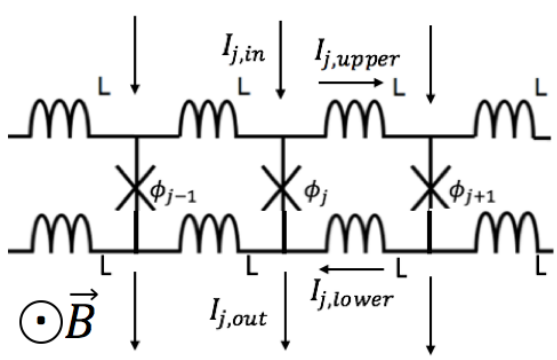

Figure 2.7. Schematic of a JJ transmission line.

Using the current labels as shown in Figure 2.7, we can apply Kirchhoff's current conservation law to the nodes above and below the jth JJ, respectively:

$$\begin{aligned} I_c \sin\phi_j + \frac{V_j}{R} + C\frac{dV_j}{dt} &= I_{j,in} - I_{j,upper} + I_{j-1,upper} = I_{j,out} - I_{j,lower} + I_{j-1,lower} \\ &\equiv \frac{I_{j,in} + I_{j,out}}{2} + \frac{(I_{j-1,upper} + I_{j-1,lower}) - (I_{j,upper} + I_{j,lower})}{2}. \end{aligned} \tag{2.14}$$

The voltage V_j can be eliminated in favor of the Josephson phase, ϕ_j, by using equation (2.2):

$$V_j = \frac{\Phi_0}{2\pi}\dot{\phi}_j, \tag{2.15}$$

wherein Φ_0 is the superconducting flux quantum.

Next, the currents flowing through the upper/lower branches can be eliminated by using the fact that the line integral of the phase difference around a closed loop on the superconductor must equal the magnetic flux enclosed by the loop. Thus, for the cell bounded by the jth and $(j+1)^{\text{st}}$ JJs, we have

$$\phi_{j+1} - \phi_j = -2\pi\frac{\Phi_j}{\Phi_0}, \tag{2.16}$$

wherein Φ_j is the total flux through the cell coming out of the paper. This total flux the sum of the flux created by the currents in the upper/lower branches, and that due to any externally applied magnetic field (with uniform flux Φ_{ext} per cell at the scale of the Josephson array):

$$\Phi_j = \Phi_{ext} - L(I_{j,upper} + I_{j,lower}). \tag{2.17}$$

Using equation (2.15) to eliminate V from equation (2.14), and using equations (2.17) and (2.16) to eliminate branch currents from equation (2.14), and rescaling time by the inverse of the 'Josephson plasma frequency', $\tau_p = \omega_p^{-1} = \sqrt{C\Phi_0/(2\pi I_c)}$, we arrive at the discrete space continuous time equation of motion governing Josephson phase evolution in the Josephson transmission line:

$$\ddot{\phi}_j + \alpha\dot{\phi}_j + \sin\phi_j = \lambda^2(\phi_{j+1} - 2\phi_j + \phi_{j-1}) + \frac{I_j}{I_c} \tag{2.18}$$

wherein $\lambda^2 = \frac{\Phi_0}{2\pi I_c L}$ controls the scale of spatial variation of the Josephson phase and $\alpha = R\sqrt{\Phi_0/(2\pi I_c C)}$ controls the dissipation. We have also replaced $(I_{j,in} + I_{j,out})/2 \to I_j$.

When $\lambda \gg 1$, the Josephson phase does not vary much from one junction to the next and we can approximate it by a smoothly varying field: $\phi_j(t) \to \phi(x,t)$. Choosing the scaling between x and j to be given by $x = j/\lambda$, the discrete second order spatial difference can be approximated by a second order spatial derivative and the field equation for ϕ becomes:

$$\phi_{tt} + \alpha\phi_t + \sin\phi = \phi_{xx} + \gamma(x,t). \tag{2.19}$$

Herein, the driving field $\gamma(x,t) = I_j(t)/I_c$ is a ratio of two terms that scale similarly with space and so is well-defined in the continuum limit.

For a lossless system and no bias current applied, equation (2.19) becomes simply the well-studied sine-Gordon equation,

$$\phi_{tt} - \phi_{xx} + \sin\phi = 0. \tag{2.20}$$

Equation (2.19) is thus the Sine-Gordon equation perturbed by terms that encode dissipation and an external driving field.

3. SOLITONS (FLUXONS) IN JJ TRANSMISSION LINES

The Sine-Gordon equation, Equation (2.20), governing the evolution of the Josephson phase along a JJ transmission line, supports novel topologically protected particle-like excitations called solitons. These are called fluxons for the specific physical case of the JJ transmission line since, as we shall see, the soliton encodes a flux quantum within itself[6].

3.1 Soliton Family of Solutions: topological protection and 'fluxons'

Solitons were first described in 1834 by John Scott Russell as he observed solitary wave in the Union canal - describing it as a "wave of translation", noting that it "continued its course along the channel apparently without change of form or diminution of speed" [25]. The wave was too large an amplitude for it to be a solution to the wave equation, which only arises as the small-amplitude approximation of the motion of water waves. This pointed to a new class of particle-like solutions existing for certain classes of nonlinear differential equations.

Solitons have since been found as solutions to a broad class of nonlinear, dispersive partial differential equations describing physical systems. Localized disturbances in dispersive media usually tend to fall apart as various frequency components travel at different speeds (nonlinear effects also influence the profile). In the unique case of solitons, the dispersion and nonlinearities compensate one another, giving rise to stable large amplitude solitary waves that propagate long distances without the form of the wave profile changing or diminishing. In addition to the sine-Gordon equation (as in equation (2.20) above), other well-studied equations that possess solitary wave solutions are the Korteweg-de Vries (KdV) equation and the nonlinear Schrödinger (NLS) equation with attractive interaction [26].

For example, the Korteweg-de Vries equation, often used to model waves on shallow water surfaces, has the form:

$$\frac{\partial u}{\partial t} + u\frac{\partial u}{\partial x} = -\frac{\partial^3 u}{\partial x^3}, \tag{3.1}$$

with a soliton solution

$$u(x,t) = 3\alpha^2 \sec\frac{1}{2}(\alpha x - \alpha^3 t), \tag{3.2}$$

which travels at a speed, α^2, that is proportional to the amplitude!

The nonlinear Schrödinger (NLS) equation with attractive interaction, which can be used to describe, for example, the dynamics of tornadoes, is

$$i\frac{\partial\Psi}{\partial t} = -\frac{1}{2m}\frac{\partial^2\Psi^2}{\partial x^2} - \lambda|\Psi|^2\Psi. \tag{3.3}$$

For $\lambda > 0$, it has solitary wave solution that appears as a knot-like kink [26]:

$$\Psi = \mathrm{e}^{i(kx-\omega t)}\sqrt{\frac{\alpha}{m\lambda}}\sec\sqrt{\alpha}(x-Ut), \tag{3.4}$$

where $k = mU$ and $\omega = \frac{1}{2}mU^2 - \frac{\alpha}{2m}$.

Finally, the general sine-Gordon (sG) equation,

$$\phi_{tt} - \phi_{xx} + \frac{m^2}{\beta}\sin\beta\phi = 0, \tag{3.5}$$

has both single- and multi-soliton solutions. The 1-soliton solution, called kink/fluxon (or antikink/antifluxon for opposite direction of propagation), represents a twist in the ϕ variable and has an exact solution of the form

$$\phi(x,t) = \frac{4}{\beta}\tan^{-1}(\mathrm{e}^{\pm m\gamma(x-Ut)}) \tag{3.6}$$

where $\gamma = \sqrt{1-U^2}$, with $|U| < 1$. These are 'topologically protected' solutions, since the phase changes from 0 ($2\pi/\beta$) at $x \to -\infty$ to $2\pi/\beta$ (0) at $x \to +\infty$. What this means is that if one slowly modifies the sine-Gordon equation to something like the the dissipative-driven equation (2.19) with the kink/antikink solution as a starting state of the field, the solution would have to persist to match the nontrivial long distance boundary conditions which require the the sine-Gordon phase ϕ to change by $\pm 2\pi/\beta$ between $x = \pm\infty$.

Not all soliton solutions are 'topologically' protected against modifications to the sine-Gordon equation. For example, an exact soliton solution of the sine-Gordon equation is the 'breather' [27], [28], the coupling of a kink and an antikink,

$$\phi(x,t) = 4\tan^{-1}\left(\frac{\sqrt{1-\omega^2}\cos\omega t}{\omega\cosh(\sqrt{1-\omega^2}x)}\right). \tag{3.7}$$

This is a nonlinear wave in which is localized and oscillatory. The breather is not topologically protected as the boundary conditions are zero, and can decay to a trivial null state if, say, dissipation is introduced.

The sG equation can be used to describe many systems including the evolution of light pulses whose frequency is in resonance with an atomic transition in the propagation medium [26]. Herein, I will use it to model the behavior of the JJ transmission lines, using the continuum limit equations (2.19) and (2.20) above. Specifically, 'topologically protected' soliton solutions of the continuum model will survive in the discrete limit, equation (2.18). The continuum limit allows one to take advantage of the fact that the pristine sine-Gordon equation is exactly solvable and dissipation/driving can be perturbatively incorporated.

Finally, we note that a single kink (antikink) soliton in the JJ transmission line requires the Josephson phase to change by $\pm 2\pi$ from left to right (note that here $\beta = 1$). However, using the analysis in equations (2.12) and (2.16), it is clear that ± 1 superconducting flux quantum is associated with the kink/antikink solution. It is for this reason that single solitons, propagating through the JJ transmission line, are call 'fluxons' and form the basis for encoding ballistic bits moving about in ABRC networks interconnected by such JJ transmission lines. From this point onward, I will use the terms 'fluxon' and 'soliton' interchangeably.

3.2 The Sine-Gordon Equation With Dissipation and Driving

The pristine sine-Gordon equation, equation (2.20), is exactly solvable. However, this is not the case when the system is perturbed with losses or driving forces, equation (2.19). I will outline below some general methods for analyzing the perturbed sG equation, equation (2.19).

3.2.1 Formal Perturbative Expansion

In this section, I will present a formal method to generate perturbative 2π-kink solutions to the perturbed sG equation, equation (2.19), using a series expansion, as done in [29]. This method can be used in the presence of dissipation and a uniform driving term and

generates traveling solutions. While the method will systematically generate a new solution, the physical content is hard to intuit and so readers looking for physical insight can skip ahead to the next subsection for a Hamiltonian-based approach.

Consider the following general form of the sine-Gordon equation:

$$\phi_{xx}(x,t) - \phi_{tt}(x,t) - \sin\phi(x,t) = \epsilon Q(x,t) \tag{3.8}$$

with Q being an operator containing all perturbative terms (assumed small) and ϵ is introduced by hand for analytic control. We will assume the existence of ballistic solutions that depend only on $\eta = x - vt$, i.e., $\phi(x,t) \equiv \phi(\eta)$ (using the same symbol for the two functions for brevity) and assume that Q is such that with this substitution, it is also a function only of η: $Q(x,t) \equiv Q(\eta)$. Clearly this is true when the dissipative term is included from equation (2.19), and if the driving term is independent of x. With this substitution, the general sine-Gordon equation becomes:

$$(1-v^2)\phi^{''}(\eta) - \sin\phi(\eta) = \epsilon Q(\eta). \tag{3.9}$$

We now seek solutions to the above equation as a series expansion in ϵ:

$$\phi(\eta) = \phi_0(\eta) + \epsilon\phi_1(\eta) + \epsilon^2\phi_2(\eta) + O(\epsilon^3) + \dots \tag{3.10}$$

The plan is to substitute this expansion into equation (3.9) and match the coefficients of powers of ϵ on both sides. For brevity, I will consider only the dissipative term: $Q = \alpha\phi_t \equiv -\alpha v\phi'(\eta)$. Using this form of Q and the expansion, equation (3.10), in equation (3.9), equating coefficients of the same power of ϵ on both sides, we find a sequence of successively solvable differential equations for ϕ_0, ϕ_1, ϕ_2, etc. [29]:

$$(1-v^2)\phi_0'' - \sin\phi_0 = 0, \tag{3.11}$$

$$(1-v^2)\phi_1' - \phi_1\cos\phi_0 + \alpha v\phi_0' = 0, \tag{3.12}$$

$$(1-v^2)\phi_2'' + \alpha v\phi_1' - \phi_2\cos\phi_0 + \frac{1}{2}\phi_1^2\sin\phi_0 = 0, \tag{3.13}$$

and so on.

An exact solution to equation (3.11), which is just the unperturbed sine-Gordon equation, is just

$$\phi_0 = 4\tan^{-1} \mathrm{e}^{\frac{\eta}{\sqrt{1-v^2}}}. \tag{3.14}$$

This can now be input into equation (3.12) to generate the solution for ϕ_1 with null boundary conditions, then both solutions for $\phi_{0,1}$ entered into equation (3.13) to generate the solution for ϕ_2 with null boundary conditions, and so on to finally generate a perturbative solution for the kink solution for the sine-Gordon equation with dissipation. While systematic, it is difficult to intuit how the perturbations modify the soliton shape or motion. This goal is better achieved by looking at energy dynamics below.

3.2.2 Hamiltonian Approach

Consider first the unperturbed sine-Gordon equation, equation (2.20),

$$\phi_{xx} - \phi_{tt} - \sin\phi = 0. \tag{3.15}$$

Remarkably, its dynamics preserves the energy functional[30]:

$$E = \int_{-\infty}^{\infty} \left(\frac{\phi_t^2}{2} + \frac{\phi_x^2}{2} + (1 - \cos\phi) \right) dx. \tag{3.16}$$

For example, the exact fluxon solution,

$$\phi(x,t) = 4\tan^{-1} \mathrm{e}^{\frac{x-vt}{\sqrt{1-v^2}}}, \tag{3.17}$$

corresponds to the (constant) energy

$$E_0 = 8(1-v^2)^{-\frac{1}{2}}. \tag{3.18}$$

The energy functional is not conserved in the presence of dissipation and driving (equation (2.19)),

$$\phi_{xx} - \phi_{tt} - \sin\phi = \alpha\phi_t - \gamma, \tag{3.19}$$

where the right-hand-side consists of the energy dissipation and uniform bias current injection terms, respectively. These terms cause the energy to change with time:

$$\begin{aligned}
\frac{dE}{dt} = \int_{-\infty}^{\infty} \frac{d}{dt}\left(\frac{\phi_t^2}{2} + \frac{\phi_x^2}{2} + (1-\cos\phi)\right)\cdot dx &= \int_{-\infty}^{\infty} (\phi_t\phi_{tt} + \phi_x\phi_{xt} + \phi_t\sin\phi)\cdot dx \\
&= \phi_x\phi_t|_{-\infty}^{\infty} + \int_{-\infty}^{\infty} (\phi_t\phi_{tt} - \phi_t\phi_{xx} + \phi_t\sin\phi)\cdot dx \\
&= \int_{-\infty}^{\infty} -\phi_t(\phi_{xx} - \phi_{tt} - \sin\phi)\cdot dx \\
&= \int_{-\infty}^{\infty} -\phi_t(\alpha\phi_t - \gamma)\cdot dx \\
&= \int_{-\infty}^{\infty} (\gamma\phi_t - \alpha\phi_t^2)\cdot dx
\end{aligned} \tag{3.20}$$

Immediately we see that it is possible for a soliton to move with no net energy change, even when dissipation and driving are present. This happens at a special velocity found by substituting equation (3.17) into the RHS of equation (3.20) and setting the integral to zero:

$$|v| = \frac{1}{\sqrt{1 + (\frac{4\alpha}{\pi\gamma})^2}} = \begin{cases} \frac{\pi\gamma}{4\alpha} & \gamma \ll 1 \\ 1 & \gamma \to 1 \end{cases} \tag{3.21}$$

This is known as the 'power balance' velocity[8], [31].

Next, for weak damping and driving, we can search for a 'adiabatic' modification of the soliton solution, equation (3.17), by making the velocity time dependent. This yields a time-dependent 'energy' using equation (3.18), whose time derivative can be equated to the last expression in equation (3.20) (with the substitution of equation (3.17) with a time-dependent velocity):

$$\frac{dv}{dt} = \gamma\pi(1-v^2)^{\frac{3}{2}} - 4\alpha v(1-v^2). \tag{3.22}$$

This is a much simpler to solve ODE that describes the physical effects of small driving currents and dissipation on the fluxon's velocity [32]. It allows the calculation of how the fluxon velocity approaches the steady-state 'power balance' velocity, equation (3.21).

3.2.3 Momentum conservation

The pristine sine-Gordon equation has translational invariance. This, by Noether's theorem[33], leads to the conservation of momentum, which is found to be[30]:

$$P = -\int_{-\infty}^{\infty} \phi_x \phi_t dx. \tag{3.23}$$

Thus, the fluxon, equation (3.17), has momentum

$$P_0 = \frac{8v}{\sqrt{1-v^2}}. \tag{3.24}$$

In the presence of uniform driving and damping, the momentum is no longer conserved and changes as follows, using equation (2.19):

$$\frac{dP}{dt} = -\alpha P + 2\pi\gamma. \tag{3.25}$$

Substituting the 'adiabatic' approximation of a time-varying velocity, $v(t)$, in equation (3.24), we find

$$4\frac{dv}{dt} = \gamma\pi(1-v^2)^{\frac{3}{2}} - 4\alpha v(1-v^2), \tag{3.26}$$

whose LHS differs from equation (3.22) by a factor of 4 while the RHS is the same. Thus, while qualitatively correct, clearly additional degrees of freedom need to be considered for the 'adiabatic' deformation of the pristine fluxon solution[34].

A natural new parameter t consider is the fluxon width, in addition to the drifting position, as captured in the ansatz:

$$\phi = 4\tan^{-1}\left(\mathrm{e}^{-\frac{x-\chi(t)}{w(t)}}\right). \tag{3.27}$$

This form can now be used to variationally find the equations of motion governing the width and location. This was done in [35], with improved matching with numerical results. Due to the increased complexity of the calculations without commensurate increase in physical content, I leave it to the interested reader to pursue that reference. In what follows, I have used the aforementioned ideas for developing physical intuition, however I have depended on numerical calculations to reliably calculate JJ circuit dynamics.

4. FLUXON LOGIC AND ABRC GATES

I will now present some fluxon logic circuits, including some new ABRC gate designs culminating with the rotary gate that I helped construct.

4.1 Historical Development: Rapid Single-Flux Quanta (RSFQ) Circuits

The first implementation of logical circuits using Josephson junctions (JJs) as an active component attempted to mimic voltage state logic in the semiconductor industry. The attraction then was the ultrafast picosecond timescale switching of JJs (this can be seen from the AC Josephson effect, which yields THz winding rates at typical maximal bias voltages of a few mV). As discussed in section 2.3, underdamped JJs exhibit hysteresis and can thus be switched between 'superconducting' and 'resistive' states depending on the time course of a bias current. They therefore can be used as switches controlled through the bias current being applied to the junction - the bit state '1' can then be associated with the resistive state and '0' with the superconducting state [36]. Such ideas were explored a few decades ago, including at companies like IBM[37].

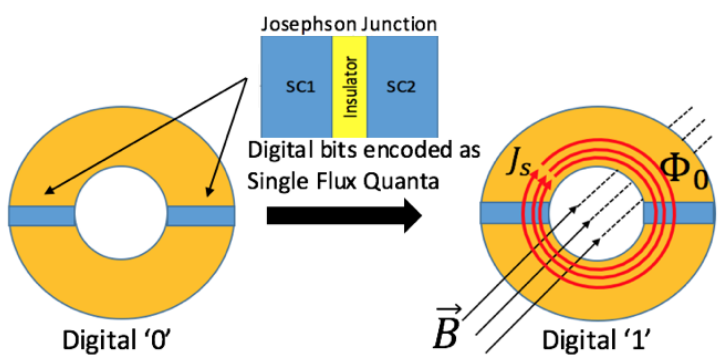

Figure 4.1. Logic in superconducting circuits is based on the presence or absence of a flux quanta (fluxons) trapped in a superconducting wire loop - the magnetic flux is quantized in the loop and digital bits can then be encoded as SFQ.

In contrast to voltage-based logical circuit families, Lihkarev and others proposed logical families that instead used the absence and presence of single flux quantum (SFQ) pulses encoded as either logical '1' or '0' [36], exploiting the topological stability of flux quanta

in superconducting rings (Figure 4.1). The information, in the form of flux quanta, is then moved around using fluxons (solitons) in analogy with propagating voltage levels through electrical circuits, as done in usual electronic computers. In this scheme, however, instead of using underdamped JJs, as was the case for the IBM example mentioned above, driven overdamped JJs (see related analysis for the 'power balance' fluxon velocity, equation (3.21)) were used to maintain tight control on fluxon propagation and eliminate oscillations (hence overdamped) [38]. Of course, such designs were inherently dissipative, an issue being addressed by designing circuits that implement asynchronous *ballistic reversible* computation (ABRC) principles, which use somewhat underdamped Josephson junctions minimize dissipation.

4.2 ABRC gate: Reversible Memory Cell Device

My collaborators at Sandia identified a circuit design demonstrating the simplest possible nontrivial asynchronous ballistic reversible computational logic functional behavior[39]. In this circuit, bits are encoded as conserved polarized fluxons in a one-bit reversible memory cell with one bidirectional I/O port. All JJs are underdamped and there is no driving current along the JJ lines. The gate circuit schematic and my numerical simulation of its behaviors are shown in Figure 4.2. A long Josephson junction transmission line (broken into 5 sections with 20 cells each, see section 3) is terminated at the reversible memory cell at the right end. The memory cell is just a JJ in a loop with inductance, L, tuned such that $LI_c \sim \Phi_0$. The physical import is that the cell can be initialized to only trap at most one fluxon/antifluxon and no more. Thus, if an incoming fluxon has the same sign as the fluxon stored in the RM cell, it gets reflected. If one gets the coupling right between the transmission line and the RM cell (mostly an art, but can be guided by matching impedance), if the incoming fluxon has the opposite sign as the fluxon stored in the RM cell, the fluxon exchanges its polarity and is reflected back with the opposite polarity, while the stored state in the RM cell also changes sign. This is a nontrivial single-terminal gate in the ABRC context [39].

In Figure 4.2, I have shown two numerical simulations performed using the WRspice circuit simulator. The simulation on the left (right) considers what happens when a fluxon

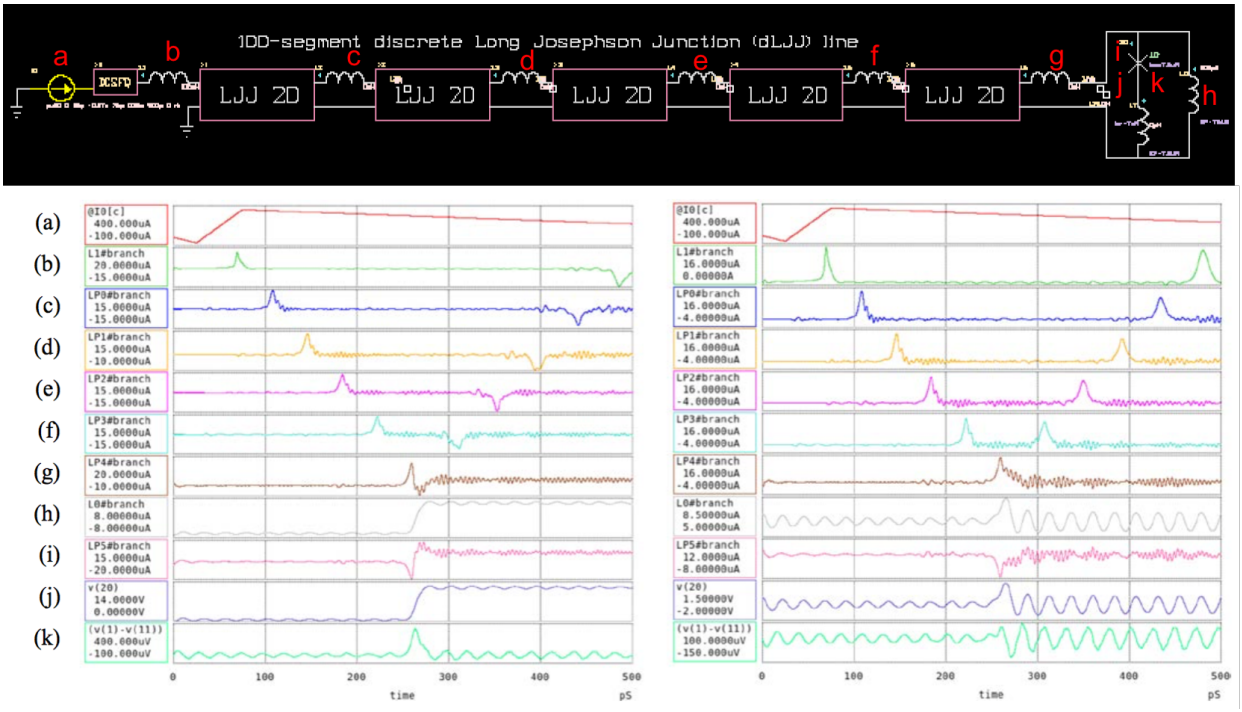

Figure 4.2. WRspice circuit schematic of Josephson Junction transmission line terminated with the reversible memory cell [39], showing my numerical calculations for two different values of the initial fluxon polarity in the storage loop (-1 and $+1$ on the left and right, respectively, relative to the propagating fluxon). (a) is a current source that generates a fluxon by rapid switching of current; (b)-(g) shows the current at each of the 6 positions indicated (these are zero inductance inductors that allow current to be recorded, an idiosyncrasy of how WRspice operates); (h) the current circulating in the terminating cell; (i) the current through the JJ in the terminating cell; (j) the JJ phase; (k) the voltage drop across the junction.

impinges on the memory cell initialized to include a fluxon of the opposite (same) sign. Let me explain what the figures show, using the analysis presented in section 2.5. Using equations (2.16) and (2.17), the spatial derivative of the Josephson phase is proportional to the currents measured in along the upper/lower superconducting lines. Using equation (3.6), it is clear that the fluxon shows up as a peaked structure in the current vs. time plot, whereas the polarity is reflected in the sign of the peak. This procedure does not give the direction of propagation; this direction is found by observing the order of appearance of the fluxon in successive points on the transmission line.

Using these insights, we now turn to interpreting my numerical calculation in Figure 4.2. It is clear from the current readings (b)–(g) that in the simulation on the left (incoming fluxon and stored fluxon have opposite signs), the fluxon is reflected with opposite polarity. The JJ phase shown in plot (j) changes by 2π such that the current flowing is equal but opposite to the initial current, showing that the stored fluxon has also changed sign (plot (h)). In the simulation on the right, when incoming and stored fluxons have the same sign, the fluxon is reflected without polarity change. The JJ phase also does not change. (The oscillations are due the underdamped nature of the junction, which ensures minimal energy loss.)

It is worth noting again the ballistic nature of the circuit, where no appreciable energy input occurs (except where the fluxon is generated in the left DCSFQ circuit) and there is little dissipation over the long process of transmission across hundreds of cells and one gate operation. The little dissipation is reflected in the slowing down and concomitant broadening of the fluxon (see dependence on v in equation (3.6)). I am collaborating with our experimental collaborators at Sandia National Laboratory to ensure successful implementation of this device.

4.3 ABRC gate: Josephson Junction Rotary Device

4.3.1 Motivation

Following the prediction of realistic circuits implementing one-terminal [39] and two-terminal [7] ABRC fluxon logic gates, let us now consider the minimal set of three-terminal devices that have been shown to be computationally universal: the rotary and toggled barrier as shown in Figure 4.3 [40].

The Rotary is a stateless 3-terminal unary (single input) device that routes pulses circularly between the terminals in a fixed rotational direction (clockwise or counterclockwise) [40]. A pulse will enter through one terminal and leave through the next terminal and so on in a cyclic fashion, the chirality being determined by the sign of the fluxon, i.e., whether it is a fluxon or an antifluxon.

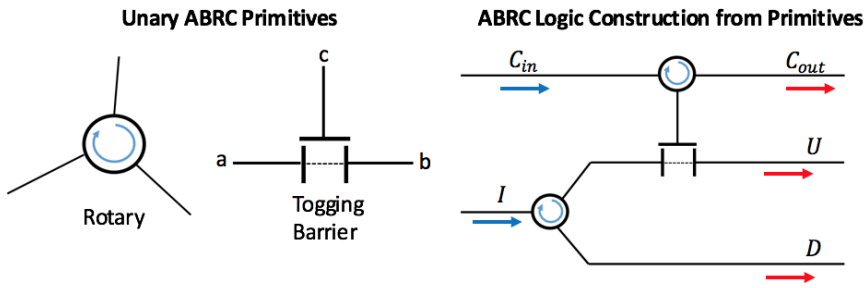

Figure 4.3. Shown on the left: minimal three-terminal ABRC devices that have been shown to be computationally universal, the Rotary and the Toggling Barrier (left). The Rotary routes a $+1$ fluxon in the direction shown and a -1 fluxon in the opposite direction. The Toggling Barrier toggles between having wire and barrier behavior in effect between its left (a) and right (b) terminals whenever a pulse reflects off its control (c) terminal. On the right is shown a possible logic gate constructed from these devices, the Toggling Switch Gate (TSG), equivalent to an AND gate. The TSG routes an incoming data signal I to either the upwards U (1) or downwards D (0) output terminal depending on which ever state is toggled by the control input C_{in} [40]. (Image credit: Dr. Michael Frank, Sandia NL.)

I have worked through some Rotary designs, the schematic of one of them shown in Figure 4.4, which did not produce the desired behavior (the fluxon got reflected irrespective of the presence and polarity of a fluxon trapped in the Rotary). We do now have a working design that works without any initialization of the rotary, presented in the next section.

4.3.2 Final Working Design of a JJ Rotary

Multiple preliminary designs from this work informed and motivated followup work spearheaded by Mr. Rishabh Khare, another graduate student in Prof. Biswas's group. Please see appendices for extensive details. Here I present the working design for the JJ Rotary developed by him, as part of this synergistic project.

The working Rotary design schematic is presented in Figure 4.5. The rotary itself is composed of three Josephson junctions, each shunting one of the three JJ transmission lines. Remarkably, even though the design looks perfectly rotationally symmetric, the polarity of

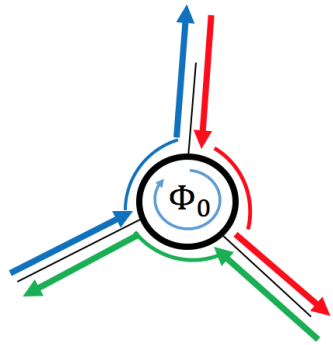

Figure 4.4. Schematic of a possible Josephson junction Rotary design that did not produce the desired behavior (the fluxons got reflected). The design had three inductances and JJs within the rotary chosen such that they could support a flux quantum at most. The thought was to mimic the behavior of the RM cell when the rotary was initialized with a stored fluxon/antifluxon, Figure 4.2, but have the incoming fluxon transmitted to a different branch. We do have a working model now, see section 4.3.2.

the incoming fluxon is sufficient to break the rotational symmetry and choose a handedness of propagation!

This is demonstrated in the propagation of a solitary fluxon coming in from the left branch, see Figure 4.6 to follow the propagating ballistic anti-fluxon (hence the sign of the current peak, note the directions of arrows in Figure 4.5 labeling current measurement directions). It is evident from the current plots that this anti-fluxon is propagating anticlockwise through the rotary. The ends of the JJ transmission lines reflect the fluxons with very little energy change and so multiple transits can be observed in Figure 4.6. Not shown here, the a fluxon with the same energy travels in the clockwise direction.

As we try to develop a physical understanding of this process in such a simple and elegant circuit, from our simulations it is clear that the chirality breaking is a function of the energy of the fluxon. There appears to be two energy thresholds. Fluxons traveling below the lowest energy threshold are simply absorbed by the rotary! Between the two energy thresholds, the antifluxons/fluxons traverse the rotary clockwise/anticlockwise, while above the higher energy threshold, the opposite behavior happens, i.e., antifluxons/fluxons traverse

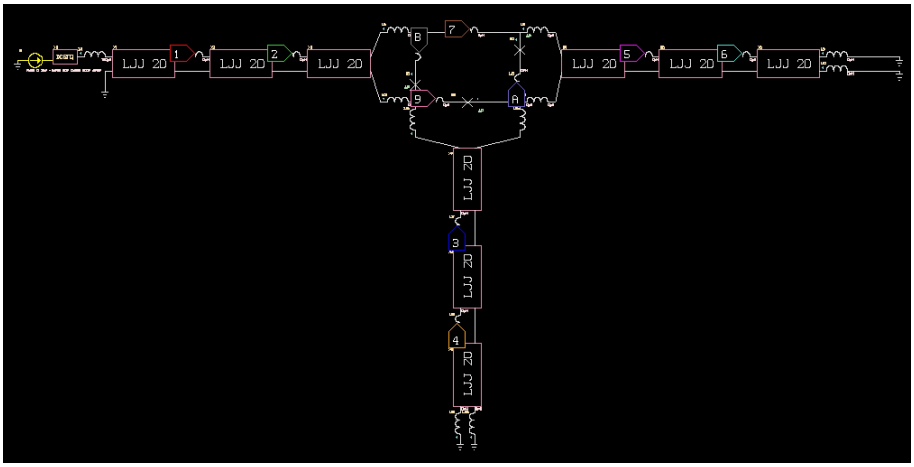

Figure 4.5. Final design for a working JJ rotary. The rotary itself is composed of three Josephson junctions, each shunting one of the three JJ transmission lines. This rotary routes antifluxons/fluxons of high enough energy in an anti-clockwise/clockwise fashion, as demonstrated for the antifluxon (magnetic flux into the paper, clockwise circulation of supercurrents) case in Figure 4.6. The large arrows correspond to the location and polarity of currents being reported over the successive graphs in Figure 4.6. (Image credit: Rudro Biswas.)

the rotary in the anticlockwise/clockwise direction. It is the last of these three regimes that has been demonstrated in Figure 4.6.

4.3.3 Summary and Future Outlook

We have thus demonstrated a working Rotary device and are developing a parameter space of its behaviors. In the long term, it is hoped that with the physical understanding gained from designing such devices, we can develop a straightforward and elegant lumped-element picture of ballistic fluxon circuits analogous to the well-developed theory of electric circuits.

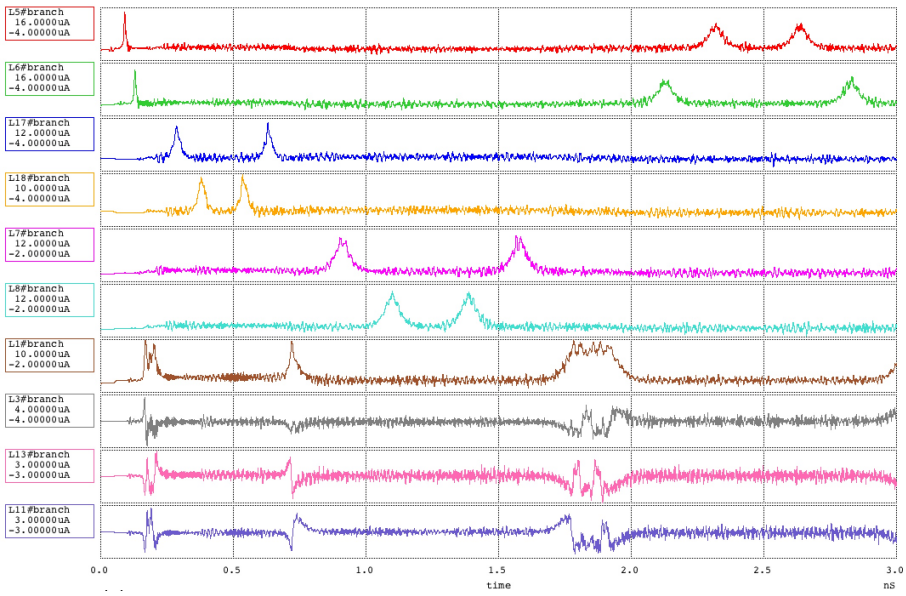

Figure 4.6. Plots of currents measured at the labeled locations of the rotary Figure 4.6. The presence of a positive peak corresponds to an antifluxon (flux directed into the paper in Figure 4.6). Clearly, this antifluxon travels anti-clockwise from the left branch to the bottom, to the right, and finally back to the left branch. In each branch, the soliton gets elastically reflected when incident at the far end. (Image credit: Rudro Biswas.)

REFERENCES

[1] M. P. Frank, R. M. Lewis, N. A. Missert, M. A. Wolak, and M. D. Henry, "Asynchronous ballistic reversible fluxon logic," *IEEE Transactions on Applied Superconductivity*, vol. 29, no. 5, pp. 1–7, 2019. DOI: 10.1109/TASC.2019.2904962.

[2] C. H. Bennett, "The thermodynamics of computation—a review," *International Journal of Theoretical Physics*, vol. 21, no. 12, pp. 905–940, 1982. DOI: 10.1007/BF02084158. [Online]. Available: https://doi.org/10.1007/BF02084158.

[3] E. Fredkin and T. Toffoli, "Conservative logic," *International Journal of Theoretical Physics*, vol. 21, no. 3, pp. 219–253, 1982. DOI: 10.1007/BF01857727. [Online]. Available: https://doi.org/10.1007/BF01857727.

[4] N. Takeuchi, Y. Yamanashi, and N. Yoshikawa, "Reversible logic gate using adiabatic superconducting devices," *Scientific Reports*, vol. 4, no. 1, p. 6354, 2014. DOI: 10.1038/srep06354. [Online]. Available: https://doi.org/10.1038/srep06354.

[5] A. Herr. "Rapid single flux quantum logic (presentation)." (), [Online]. Available: https://terpconnect.umd.edu/~kosborn/index_files/SEALeR/Anna%20Herr.pdf.

[6] T. Fulton, R. Dynes, and P. Anderson, "The flux shuttle—a josephson junction shift register employing single flux quanta," *Proceedings of the IEEE*, vol. 61, no. 1, pp. 28–35, 1973. DOI: 10.1109/PROC.1973.8966.

[7] W. Wustmann and K. D. Osborn, "Reversible fluxon logic: Topological particles allow ballistic gates along one-dimensional paths," *Phys. Rev. B*, vol. 101, p. 014 516, 1 Jan. 2020. DOI: 10.1103/PhysRevB.101.014516. [Online]. Available: https://link.aps.org/doi/10.1103/PhysRevB.101.014516.

[8] N. Pedersen, "Fluxon electronic devices," *IEEE Transactions on Magnetics*, vol. 27, no. 2, pp. 3328–3334, 1991. DOI: 10.1109/20.133925.

[9] H. Onnes and W. Keesom, "The superconductivity of mercury.," *Commun. Phys. Lab. Univ. Leiden. Suppl. 29*, 1911.

[10] S. J. Singh and P. Mele, "Future potential of new high tc iron-based superconductors," in *Superconductivity: From Materials Science to Practical Applications*, P. Mele, K. Prassides, C. Tarantini, *et al.*, Eds. Cham: Springer International Publishing, 2020, pp. 243–267, ISBN: 978-3-030-23303-7. DOI: 10.1007/978-3-030-23303-7{_}9. [Online]. Available: https://doi.org/10.1007/978-3-030-23303-7_9.

[11] W. Meissner and R. Ochsenfeld, "Ein neuer effekt bei eintritt der supraleitfähigkeit," *Naturwissenschaften*, vol. 21, no. 44, pp. 787–788, 1933. DOI: 10.1007/BF01504252. [Online]. Available: https://doi.org/10.1007/BF01504252.

[12] V. L. Ginzburg and L. D. Landau, *Zh. Eksp. Teor. Fiz.*, vol. 20, p. 1064, 1950.

[13] V. L. Ginzburg, "Nobel lecture: On superconductivity and superfluidity (what i have and have not managed to do) as well as on the "physical minimum" at the beginning of the xxi century," *Rev. Mod. Phys.*, vol. 76, pp. 981–998, 3 Dec. 2004. DOI: 10.1103/RevModPhys.76.981. [Online]. Available: https://link.aps.org/doi/10.1103/RevModPhys.76.981.

[14] J. Bardeen, L. N. Cooper, and J. R. Schrieffer, "Theory of superconductivity," *Phys. Rev.*, vol. 108, pp. 1175–1204, 5 Dec. 1957. DOI: 10.1103/PhysRev.108.1175. [Online]. Available: https://link.aps.org/doi/10.1103/PhysRev.108.1175.

[15] B. Josephson, "Possible new effects in superconductive tunnelling," *Physics Letters*, vol. 1, no. 7, pp. 251–253, 1962, ISSN: 0031-9163. DOI: https://doi.org/10.1016/0031-9163(62)91369-0. [Online]. Available: https://www.sciencedirect.com/science/article/pii/0031916362913690.

[16] P. W. Anderson and J. M. Rowell, "Probable observation of the josephson superconducting tunneling effect," *Phys. Rev. Lett.*, vol. 10, pp. 230–232, 6 Mar. 1963. DOI: 10.1103/PhysRevLett.10.230. [Online]. Available: https://link.aps.org/doi/10.1103/PhysRevLett.10.230.

[17] M. Tinkham, *Introduction to superconductivity*, 2nd ed. New York: McGraw Hill, 1996, ISBN: 0070648786. [Online]. Available: http://www.loc.gov/catdir/description/mh022/95022378.html.

[18] B. D. Josephson, "Coupled superconductors," *Rev. Mod. Phys.*, vol. 36, pp. 216–220, 1 Jan. 1964. DOI: 10.1103/RevModPhys.36.216. [Online]. Available: https://link.aps.org/doi/10.1103/RevModPhys.36.216.

[19] R. Gross, A. Marx, and F. Deppe, *Applied Superconductivity: Josephson Effect and Superconducting Electronics* (De Gruyter Textbook Series). Walter De Gruyter Incorporated, 2016, ISBN: 9783110417067. [Online]. Available: https://books.google.com/books?id=4SIzrgEACAAJ.

[20] D. E. McCumber, "Effect of ac impedance on dc voltage-current characteristics of superconductor weak-link junctions," *Journal of Applied Physics*, vol. 39, no. 7, pp. 3113–3118, 2022/06/25 1968. DOI: 10.1063/1.1656743. [Online]. Available: https://doi.org/10.1063/1.1656743.

[21] W. C. Stewart, "Current-voltage characteristics of josephson junctions," *Applied Physics Letters*, vol. 12, no. 8, pp. 277–280, 2022/06/25 1968. DOI: 10.1063/1.1651991. [Online]. Available: https://doi.org/10.1063/1.1651991.

[22] B. S. Deaver and W. M. Fairbank, "Experimental evidence for quantized flux in superconducting cylinders," *Phys. Rev. Lett.*, vol. 7, pp. 43–46, 2 Jul. 1961. DOI: 10.1103/PhysRevLett.7.43. [Online]. Available: https://link.aps.org/doi/10.1103/PhysRevLett.7.43.

[23] R. Doll and M. Nabauer, "Experimental proof of magnetic flux quantization in a superconducting ring," *Phys. Rev. Lett.*, vol. 7, pp. 51–52, 2 Jul. 1961. DOI: 10.1103/PhysRevLett.7.51. [Online]. Available: https://link.aps.org/doi/10.1103/PhysRevLett.7.51.

[24] J. J. Mazo and A. V. Ustinov, "The sine-gordon equation in josephson-junction arrays," in *The sine-Gordon Model and its Applications: From Pendula and Josephson Junctions to Gravity and High-Energy Physics*, J. Cuevas-Maraver, P. G. Kevrekidis, and F. Williams, Eds. Cham: Springer International Publishing, 2014, pp. 155–175, ISBN: 978-3-319-06722-3. DOI: 10.1007/978-3-319-06722-3_7. [Online]. Available: https://doi.org/10.1007/978-3-319-06722-3_7.

[25] M. Remoissenet, *Waves called solitons: concepts and experiments*. Springer Science & Business Media, 2013.

[26] M. Stone and P. Goldbart, *Mathematics for physics: a guided tour for graduate students*. Cambridge University Press, 2009.

[27] G. Costabile, R. D. Parmentier, B. Savo, D. W. McLaughlin, and A. C. Scott, "Exact solutions of the sine-gordon equation describing oscillations in a long (but finite) josephson junction," *Applied Physics Letters*, vol. 32, no. 9, pp. 587–589, 2022/06/25 1978. DOI: 10.1063/1.90113. [Online]. Available: https://doi.org/10.1063/1.90113.

[28] J.-G. Caputo and D. Dutykh, "Nonlinear waves in networks: Model reduction for the sine-gordon equation," *Phys. Rev. E*, vol. 90, p. 022 912, 2 Aug. 2014. DOI: 10.1103/PhysRevE.90.022912. [Online]. Available: https://link.aps.org/doi/10.1103/PhysRevE.90.022912.

[29] A. C. Scott, F. Y. F. Chu, and S. A. Reible, "Magnetic-flux propagation on a josephson transmission line," *Journal of Applied Physics*, vol. 47, no. 7, pp. 3272–3286, 2022/06/25 1976. DOI: 10.1063/1.323126. [Online]. Available: https://doi.org/10.1063/1.323126.

[30] B. A. Malomed, "The sine-gordon model: General background, physical motivations, inverse scattering, and solitons," in *The sine-Gordon Model and its Applications: From Pendula and Josephson Junctions to Gravity and High-Energy Physics*, J. Cuevas-Maraver, P. G. Kevrekidis, and F. Williams, Eds. Cham: Springer International Publishing, 2014, pp. 1–30, ISBN: 978-3-319-06722-3. DOI: 10.1007/978-3-319-06722-3_1. [Online]. Available: https://doi.org/10.1007/978-3-319-06722-3_1.

[31] N. F. Pedersen, M. R. Samuelsen, and D. Welner, "Soliton annihilation in the perturbed sine-gordon system," *Phys. Rev. B*, vol. 30, pp. 4057–4059, 7 Oct. 1984. DOI: 10.1103/PhysRevB.30.4057. [Online]. Available: https://link.aps.org/doi/10.1103/PhysRevB.30.4057.

[32] D. W. McLaughlin and A. C. Scott, "Perturbation analysis of fluxon dynamics," *Phys. Rev. A*, vol. 18, pp. 1652–1680, 4 Oct. 1978. DOI: 10.1103/PhysRevA.18.1652. [Online]. Available: https://link.aps.org/doi/10.1103/PhysRevA.18.1652.

[33] E. Noether, "Invariante variationsprobleme," ger, *Nachrichten von der Gesellschaft der Wissenschaften zu Göttingen, Mathematisch-Physikalische Klasse*, vol. 1918, pp. 235–257, 1918. [Online]. Available: http://eudml.org/doc/59024.

[34] D. R. Gulevich and F. V. Kusmartsev, "Perturbation theory for localized solutions of the sine-gordon equation: Decay of a breather and pinning by a microresistor," *Phys. Rev. B*, vol. 74, p. 214 303, 21 Dec. 2006. DOI: 10.1103/PhysRevB.74.214303. [Online]. Available: https://link.aps.org/doi/10.1103/PhysRevB.74.214303.

[35] N. F. Smyth and A. L. Worthy, "Soliton evolution and radiation loss for the sine-gordon equation," *Phys. Rev. E*, vol. 60, pp. 2330–2336, 2 Aug. 1999. DOI: 10.1103/PhysRevE.60.2330. [Online]. Available: https://link.aps.org/doi/10.1103/PhysRevE.60.2330.

[36] K. Likharev and V. Semenov, "Rsfq logic/memory family: A new josephson-junction technology for sub-terahertz-clock-frequency digital systems," *IEEE Transactions on Applied Superconductivity*, vol. 1, no. 1, pp. 3–28, 1991. DOI: 10.1109/77.80745.

[37] T. Rajeevakumar, "A soliton device," *IEEE Transactions on Magnetics*, vol. 17, no. 1, pp. 591–594, 1981. DOI: 10.1109/TMAG.1981.1060933.

[38] L. C. Muller, "Rsfq digital circuit design automation and optimisation," Ph.D. dissertation, Stellenbosch University, 2015. [Online]. Available: https://core.ac.uk/display/37438155.

[39] M. P. Frank, R. M. Lewis, N. A. Missert, M. D. Henry, M. A. Wolak, and E. P. DeBenedictis, "Semi-automated design of functional elements for a new approach to digital superconducting electronics: Methodology and preliminary results," in *2019 IEEE International Superconductive Electronics Conference (ISEC)*, 2019, pp. 1–6. DOI: 10.1109/ISEC46533.2019.8990900.

[40] M. P. Frank, "Asynchronous ballistic reversible computing," in *2017 IEEE International Conference on Rebooting Computing (ICRC)*, 2017, pp. 1–8. DOI: 10.1109/ICRC.2017.8123659.

A. APPENDIX: JJ ROTARY - BRANCHES TERMINATED WITH RESISTORS

In this appendix, we outline our method of performing a parameter sweep on resistors added to the Josephson junction rotary device simulations in WRspice. Below shows the JJ rotary we are simulating. The incoming flux travels through the 3 rotary branch/terminals in a counter-clockwise fashion.

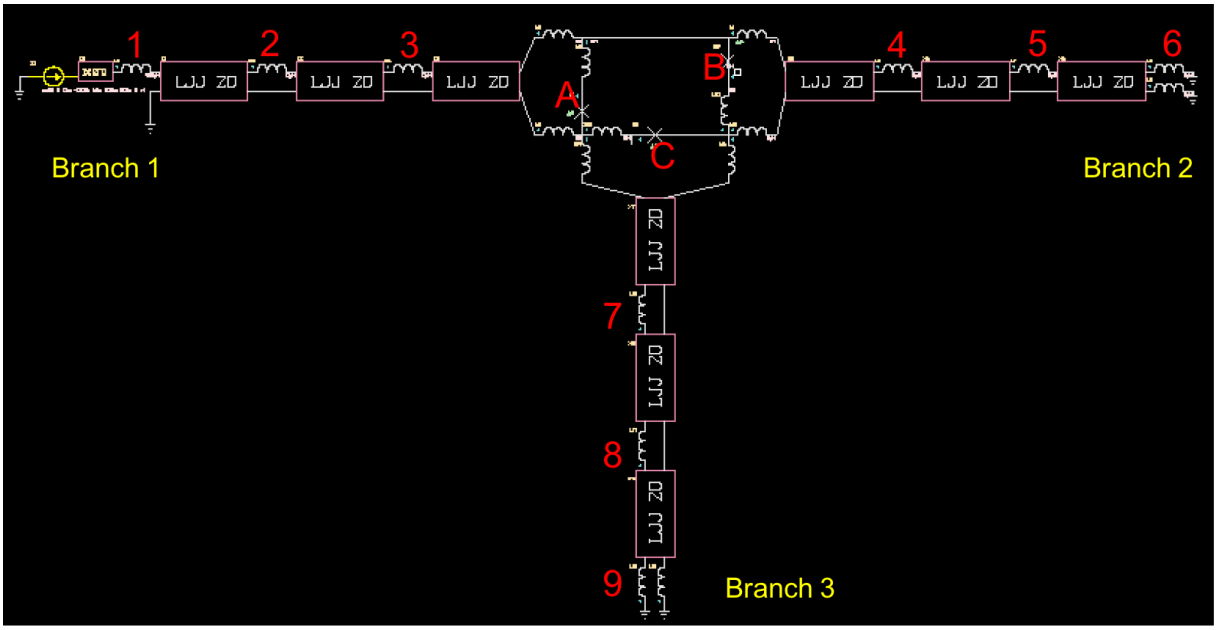

Figure A.1. Circuit schematic of Josephson Junction rotary device as seen in WRspice with each of the 3 branches indicated. Labels 1-9 correspond to the current at each location and A-C indicate the JJ phase on each of the 3 junctions.

Figure A.1 shows the JJ rotary device we are simulating.

A.1 Both Branch 2 and 3 terminated with resistor

Figure A.2 show resistors are connected to terminate each branch in WRspice. As seen in the Figures A.3 - A.5 below, both branches 2 and 3 are terminated with a resistor. A parameter sweep simulation is performed for resistance values, $R = 1\Omega$, $R = 5\Omega$, and

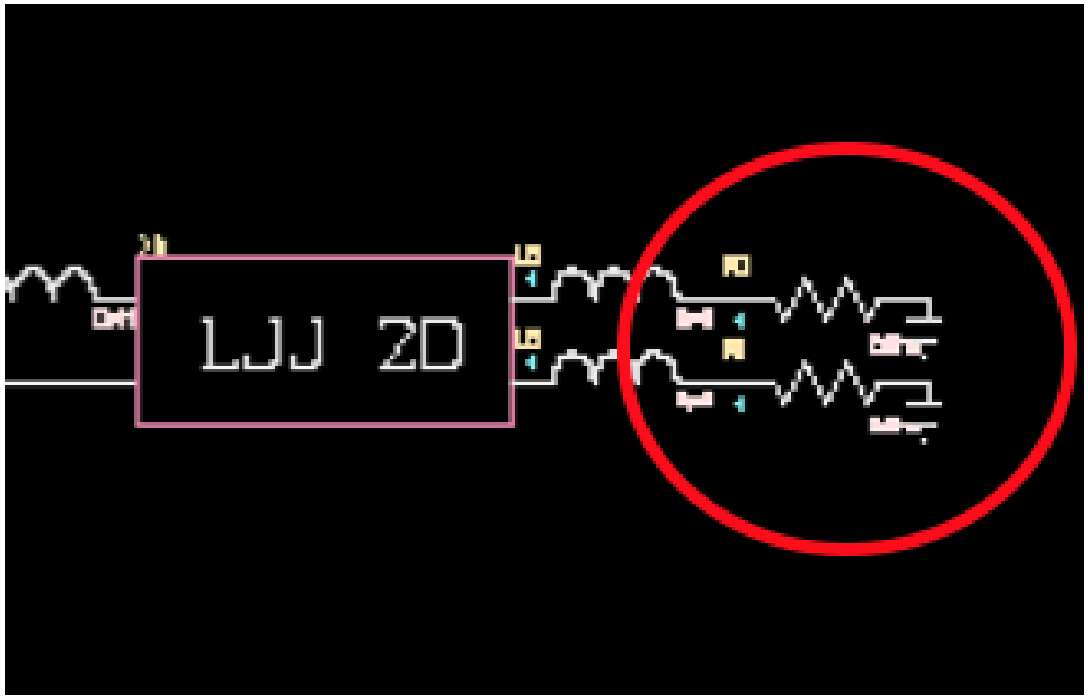

Figure A.2. JJ branches terminated with resistor.

$R = 9\Omega$. Below are the results for the parameter sweep for each resistance value with both branches terminated with the resistor.

A.2 Only Branch 2 terminated with resistor

In this section, we show simulation results when only branch 2 is terminated with a resistor. A parameter sweep is performed and the results are shown in Figures A.6-A.8.

A.3 Only Branch 3 terminated with resistor

In this section, we show simulation results when only branch 3 is terminated with a resistor. A parameter sweep is performed and the results are shown in Figures A.9-A.11.

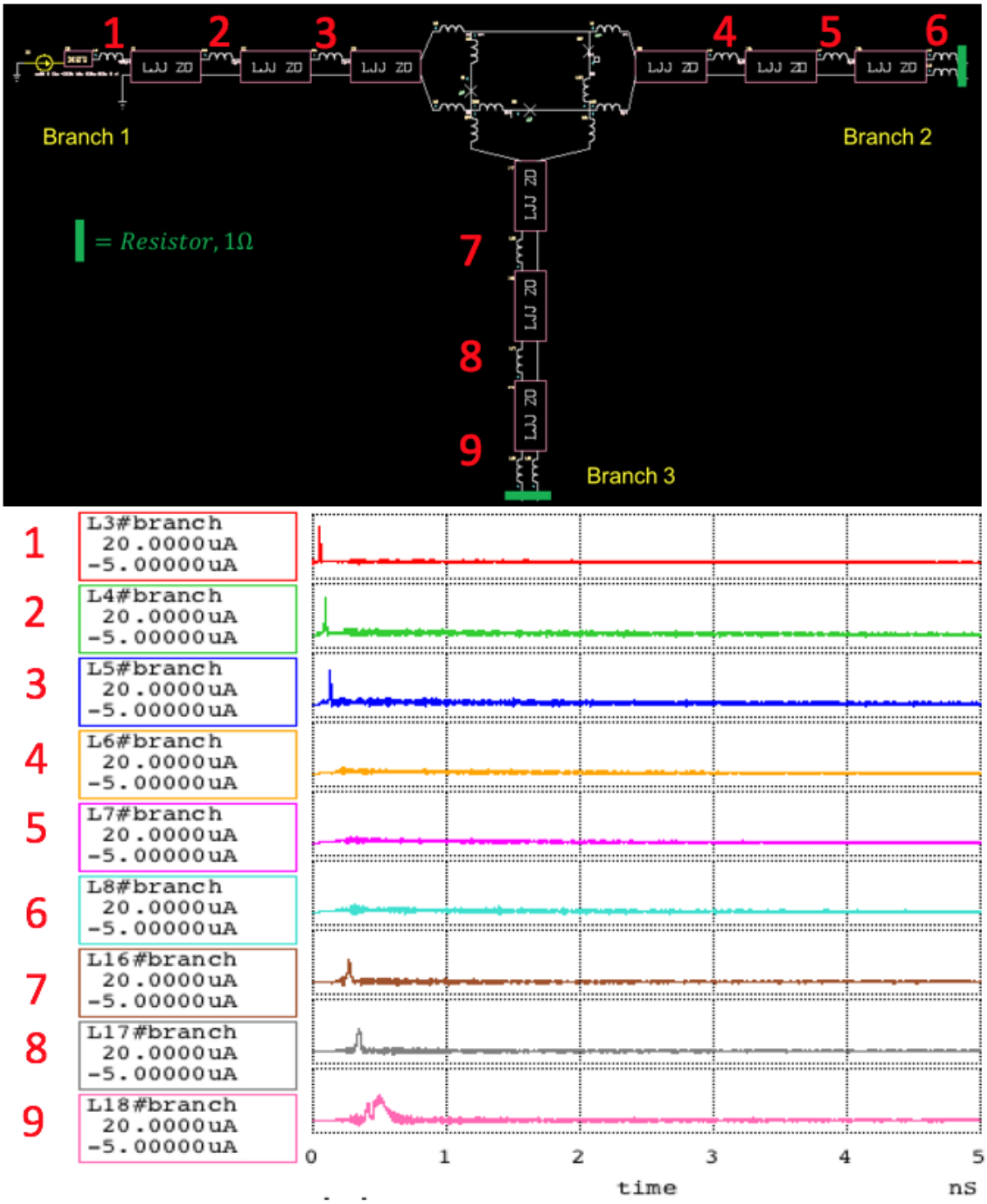

Figure A.3. Branches 2 and 3 are terminated in a 1Ω resistor. Fluxon absorbed in branch 3.

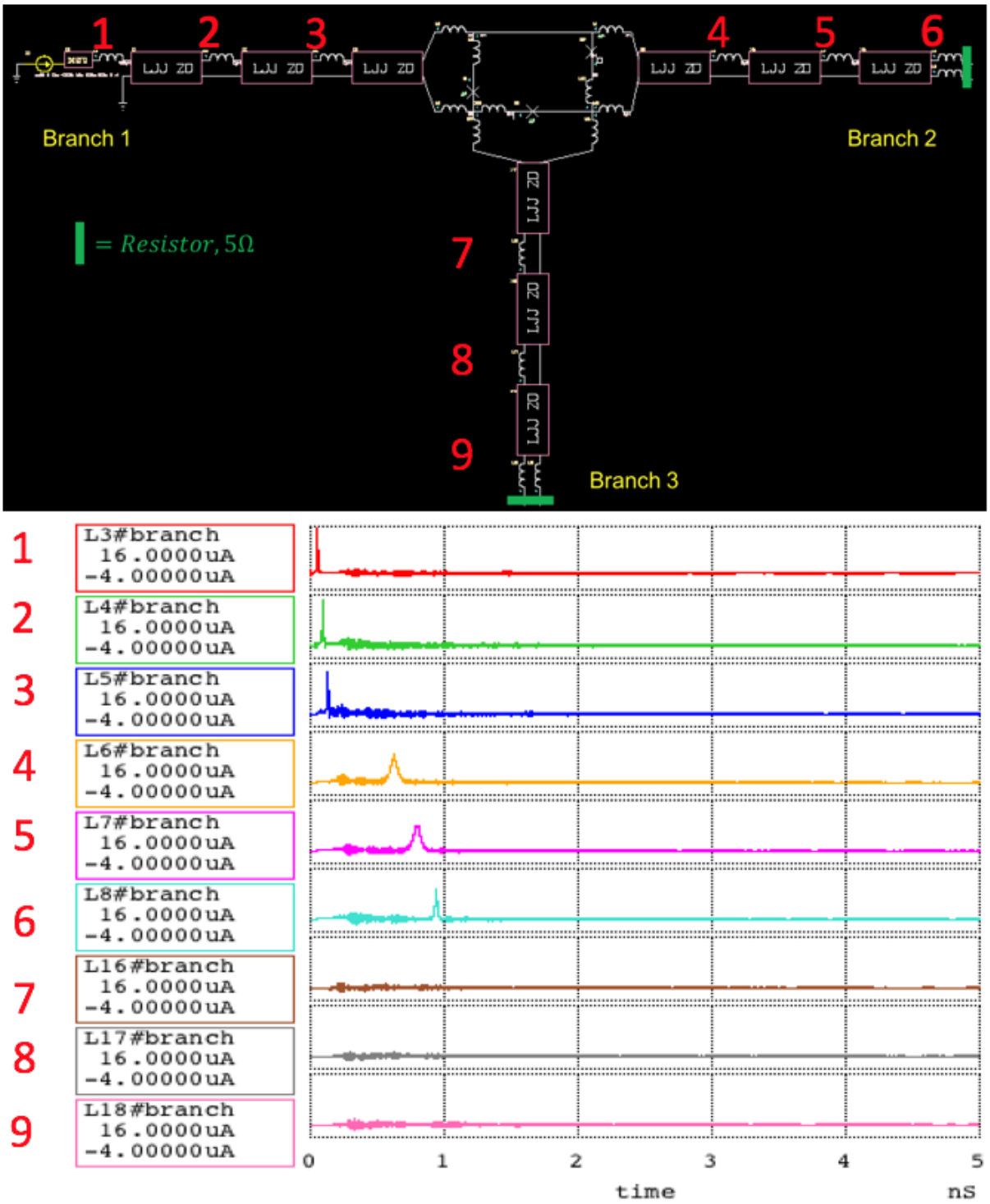

Figure A.4. Branches 2 and 3 are terminated in a 5Ω resistor. Fluxon absorbed in branch 2.

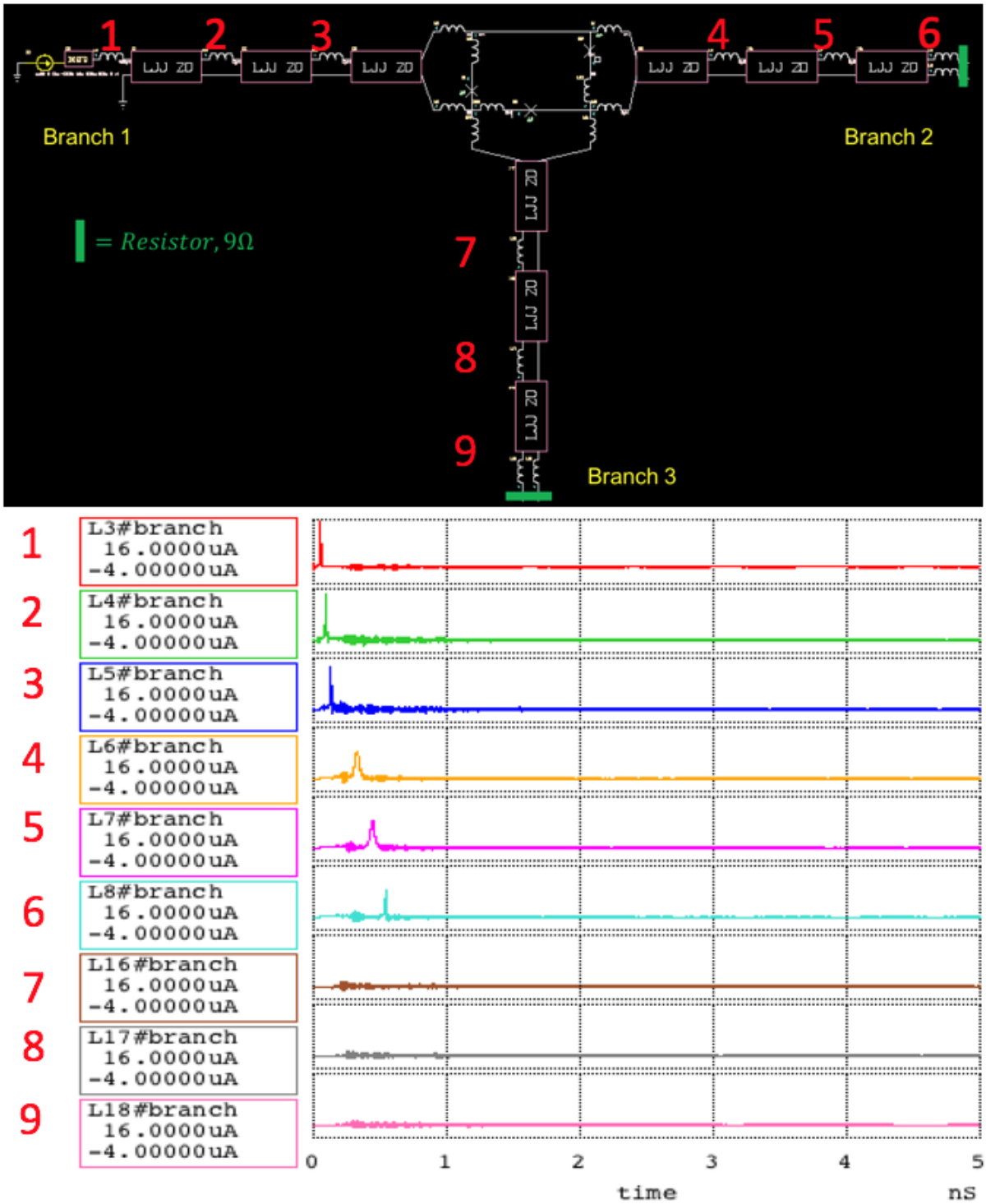

Figure A.5. Branches 2 and 3 are terminated in a 9Ω resistor. Fluxon absorbed in branch 2.

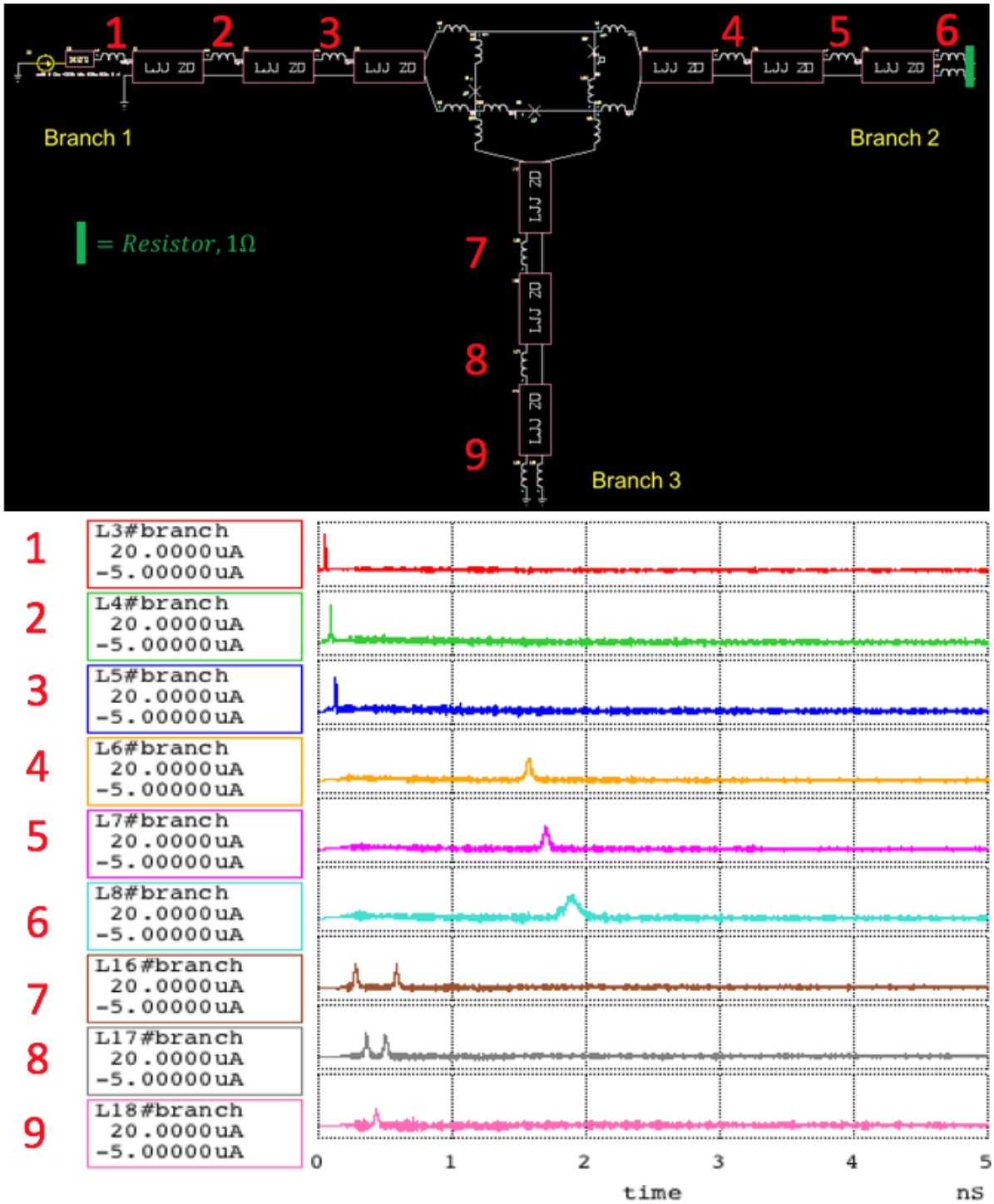

Figure A.6. Branch 2 is terminated in a 1Ω resistor. Fluxon propagates from branch 1, to branch 3 (reflected from resistor), then enters branch 2 and is absorbed in branch 2 resistor.

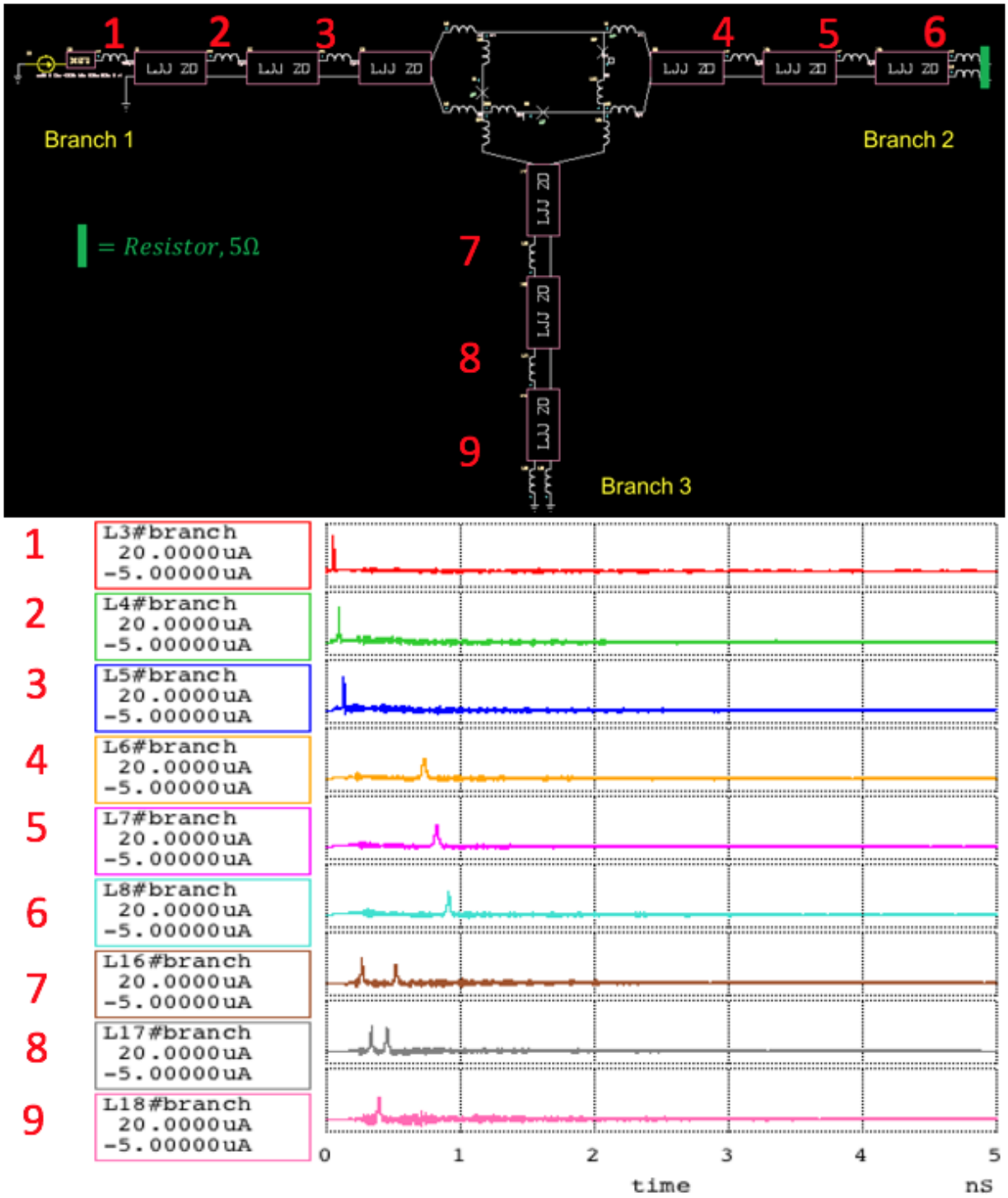

Figure A.7. Branch 2 is terminated in a 5Ω resistor. Fluxon propagates from branch 1, to branch 3 (reflected from resistor), then enters branch 2 and is absorbed in branch 2 resistor.

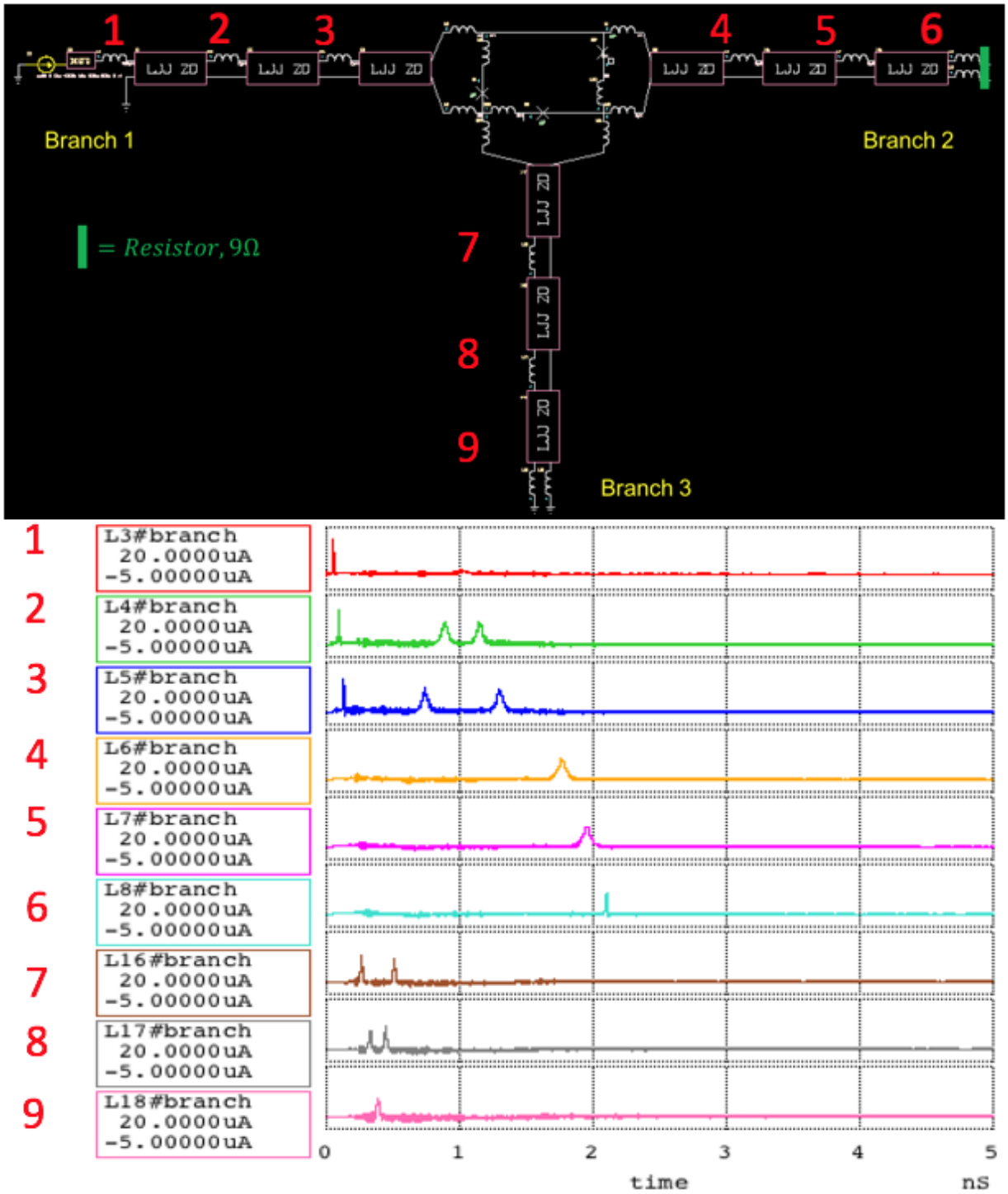

Figure A.8. Branch 2 is terminated in a 9Ω resistor. Fluxon re-enters branch 1.

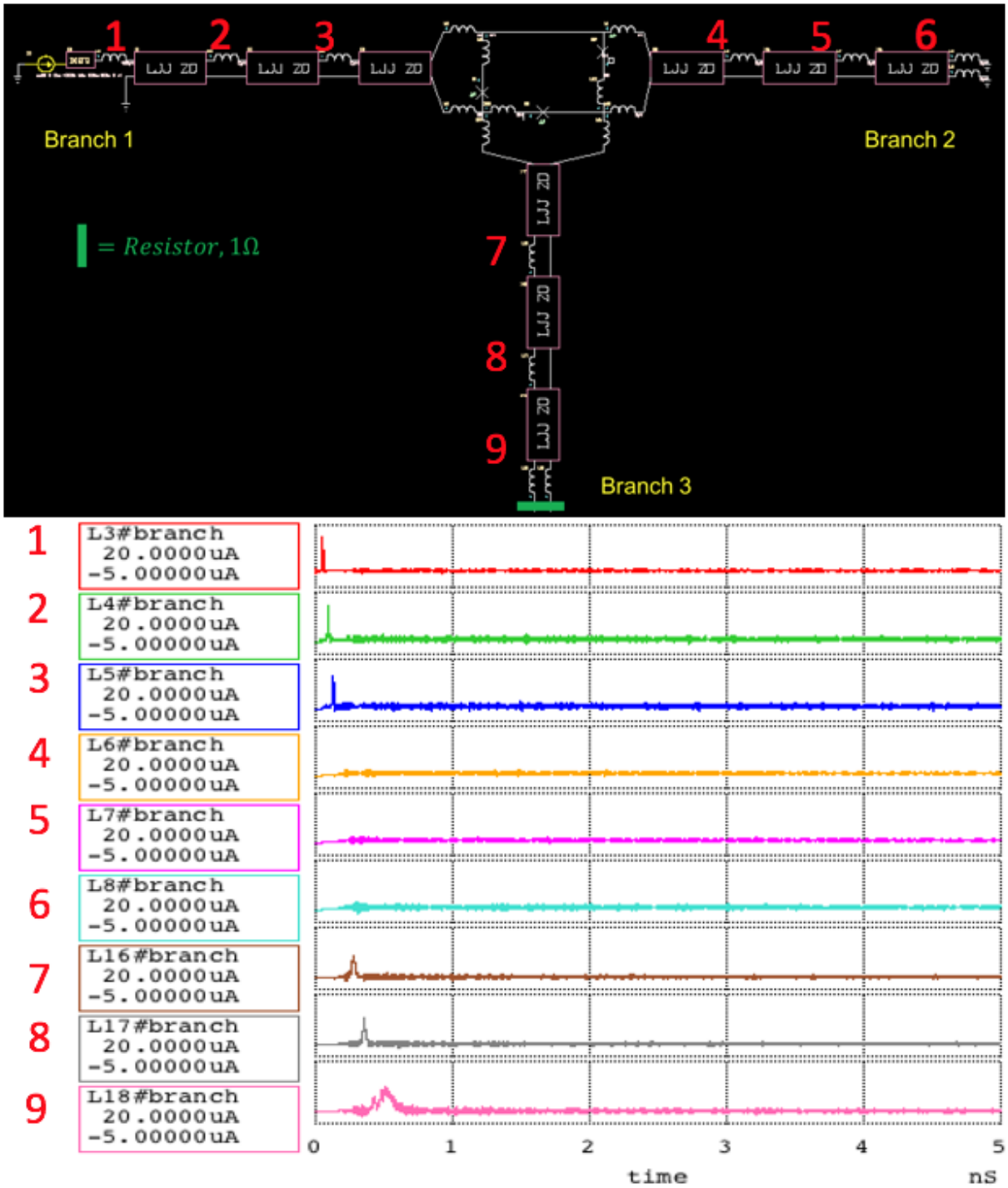

Figure A.9. Branch 3 is terminated in a 1Ω resistor. Fluxon is absorbed in branch 3. It does not enter branch 2.

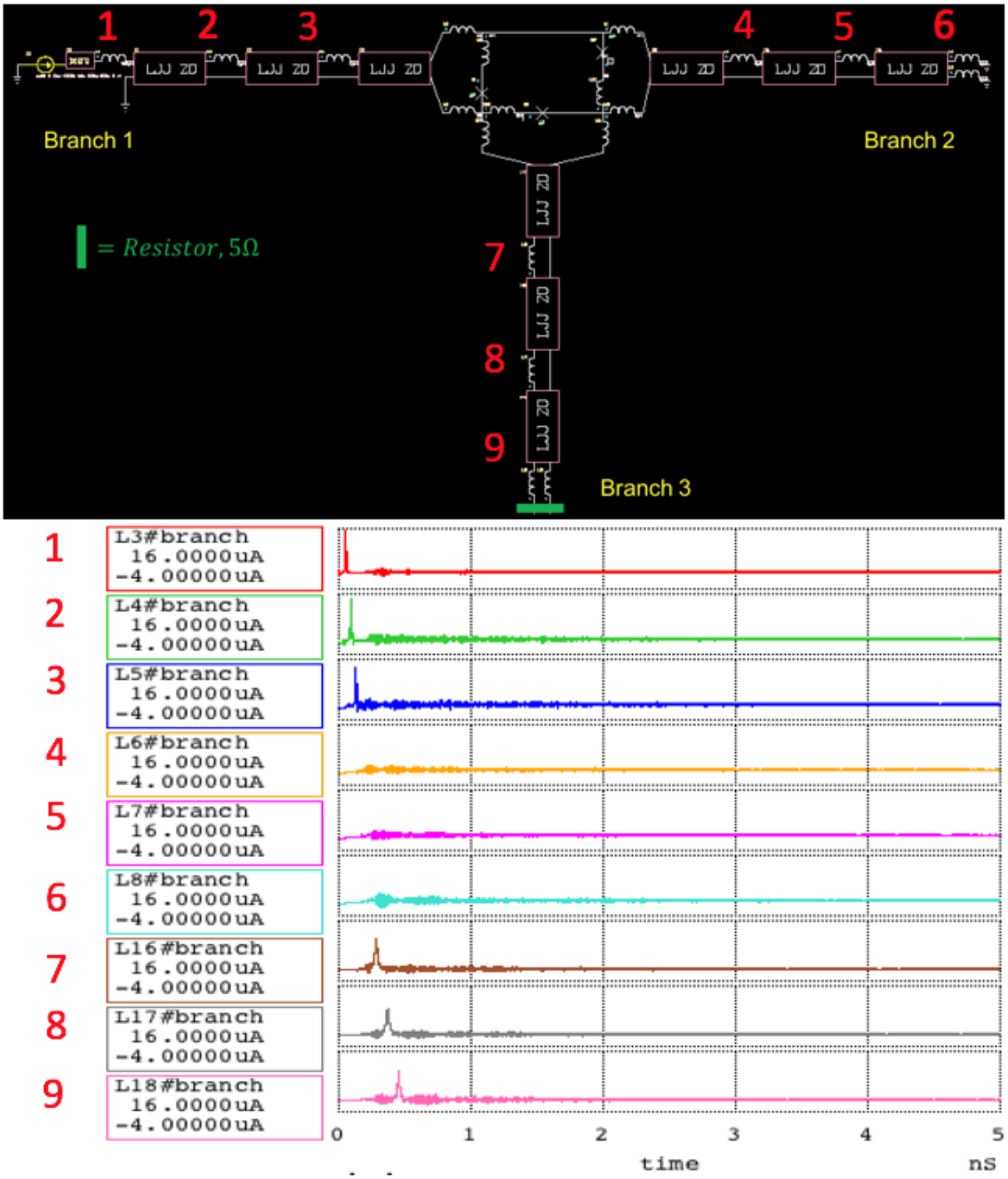

Figure A.10. Branch 3 is terminated in a 5Ω resistor. Fluxon is absorbed in branch 3. It does not enter branch 2

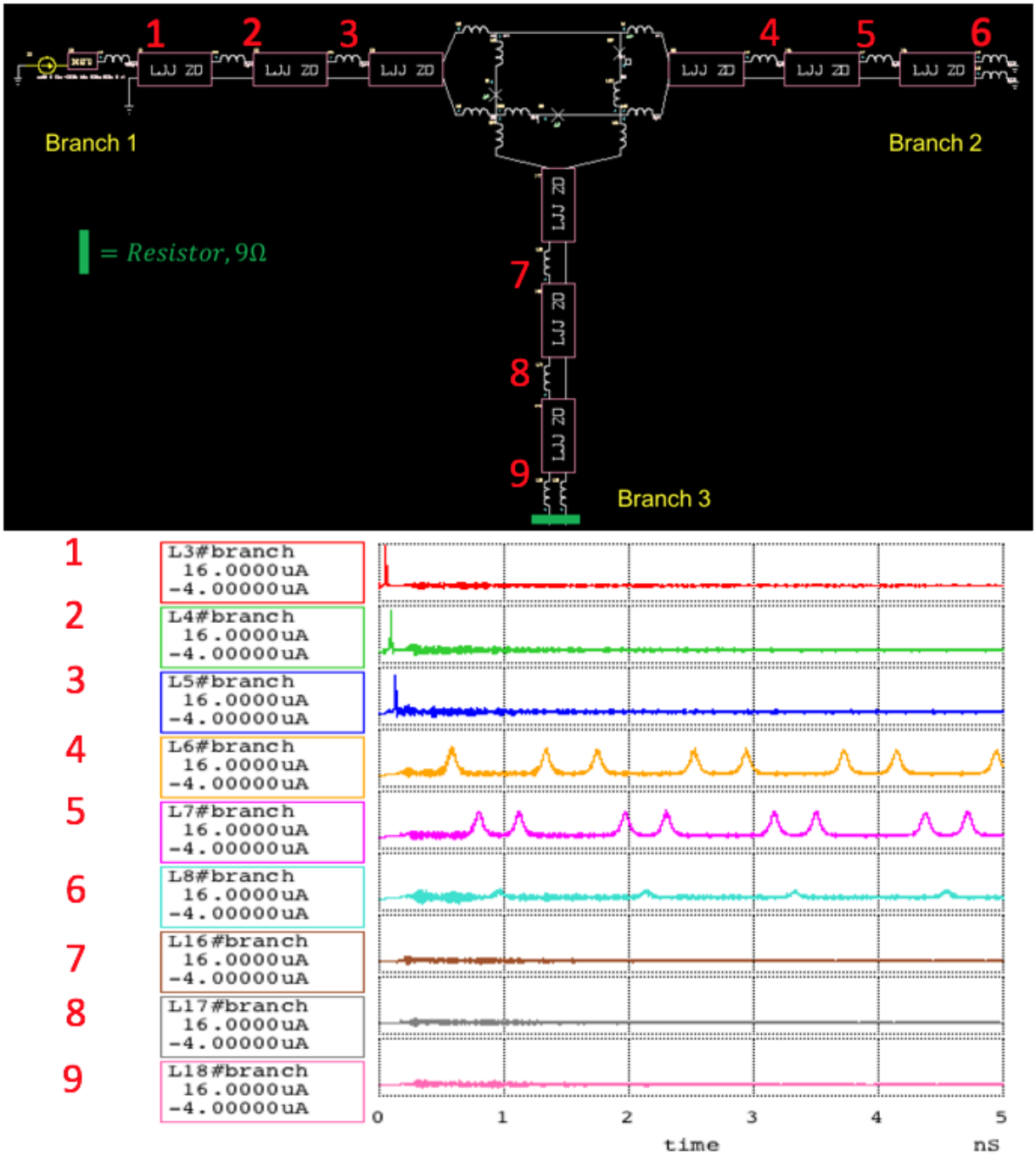

Figure A.11. Branch 3 is terminated in a 9Ω resistor. Fluxon does not enter branch 3 and is reflected repeatedly between rotary junction and branch 2 resistor.

B. APPENDIX: JJ ROTARY - CURRENT INITIALIZED IN ROTARY

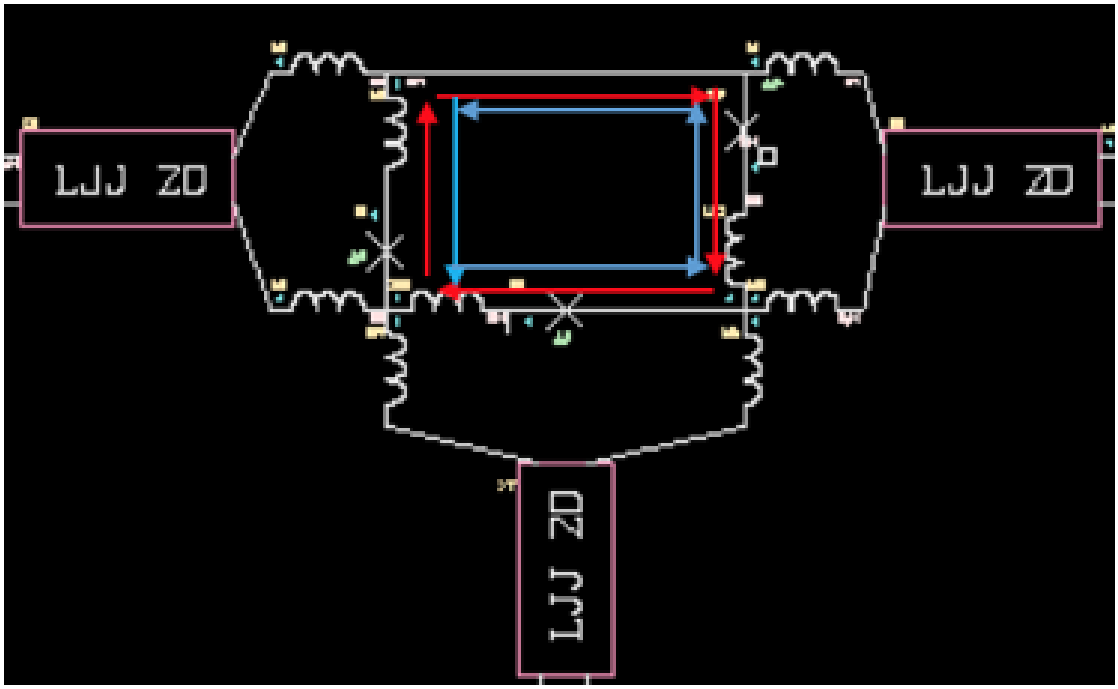

Figure B.1. Branch 3 is terminated in a 9Ω resistor.

In this appendix, we outline our method of performing a parameter sweep on an initialized current in the JJ rotary device. This is done for both clockwise and counter-clockwise configuration as seen in Figure B.1.

B.1 JJ Rotary - Clockwise Current Initialized in Rotary

In this section, we show simulation results for an initialized clockwise current in the JJ rotary device. All JJs have a critical current (CW) of $I_c = 1.5\mu A$. A parameter sweep simulation is performed for initial currents $I_0 = 0.57\mu A$, $I_0 = 1.06\mu A$, and $I_0 = 1.39\mu A$. The results are shown below in Figures B.2-B.4.

B.2 JJ Rotary - Counter-Clockwise Current Initialized in Rotary

In this section, we show simulation results for an initialized counter-clockwise current in the JJ rotary device. All JJs have a critical current of $I_c = 1.5\mu A$. A parameter sweep simulation is again performed for initial currents (CCW) $I_0 = 0.57\mu A$, $I_0 = 1.06\mu A$, and $I_0 = 1.39\mu A$. The results are shown below results are shown below in Figures B.5-B.7.

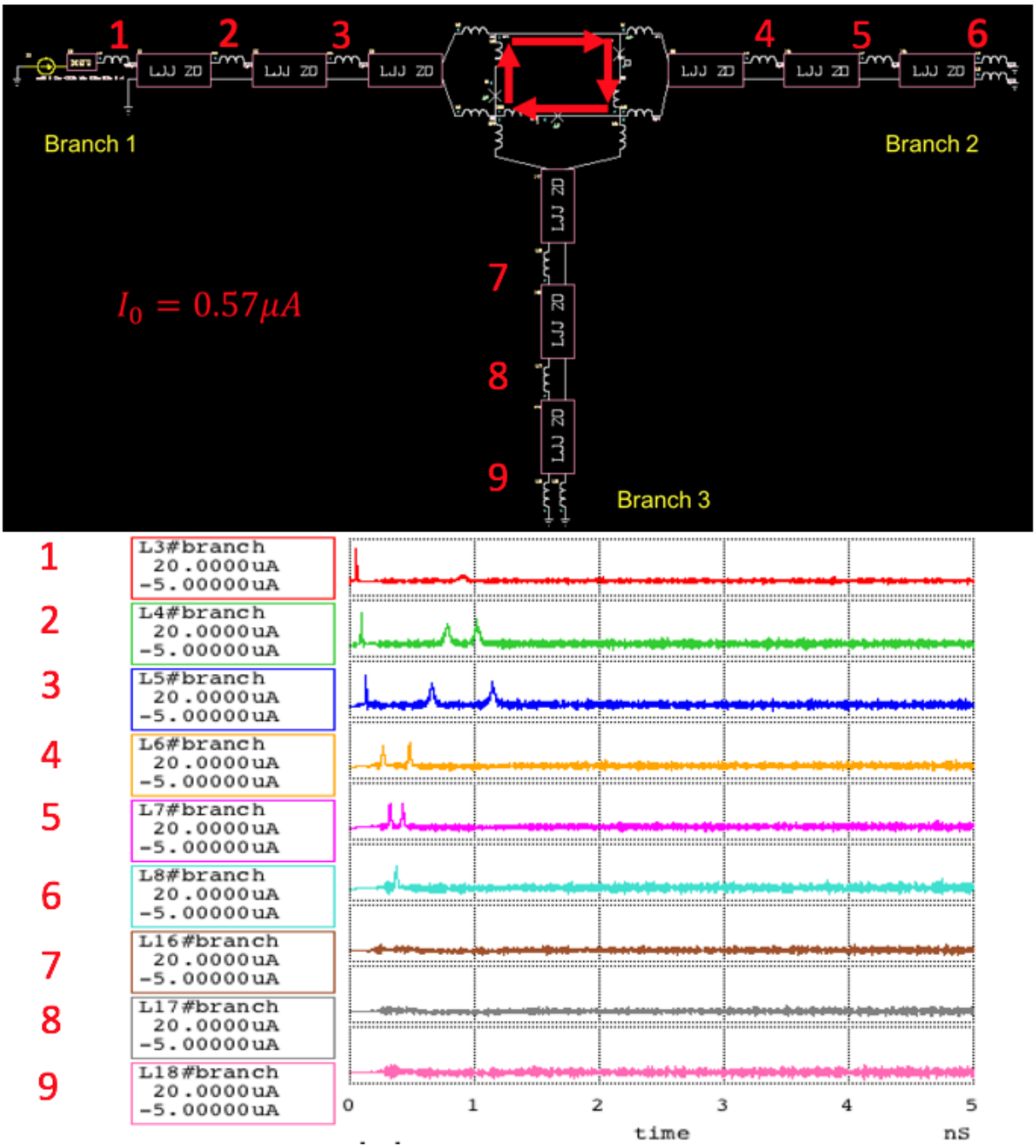

Figure B.2. Initial clockwise current of $I_0 = 0.57\mu A$

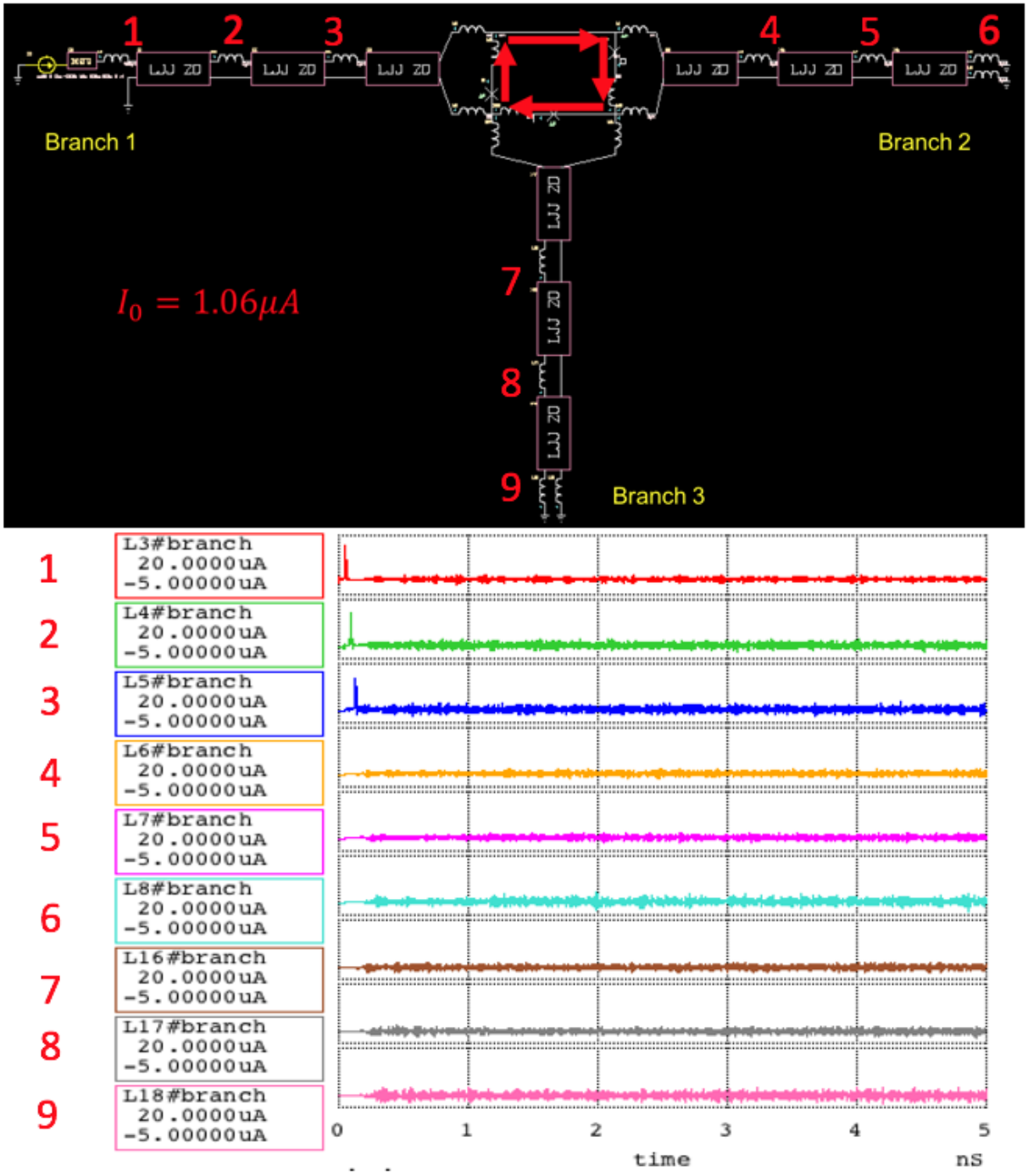

Figure B.3. Initial clockwise current of $I_0 = 1.06\mu A$

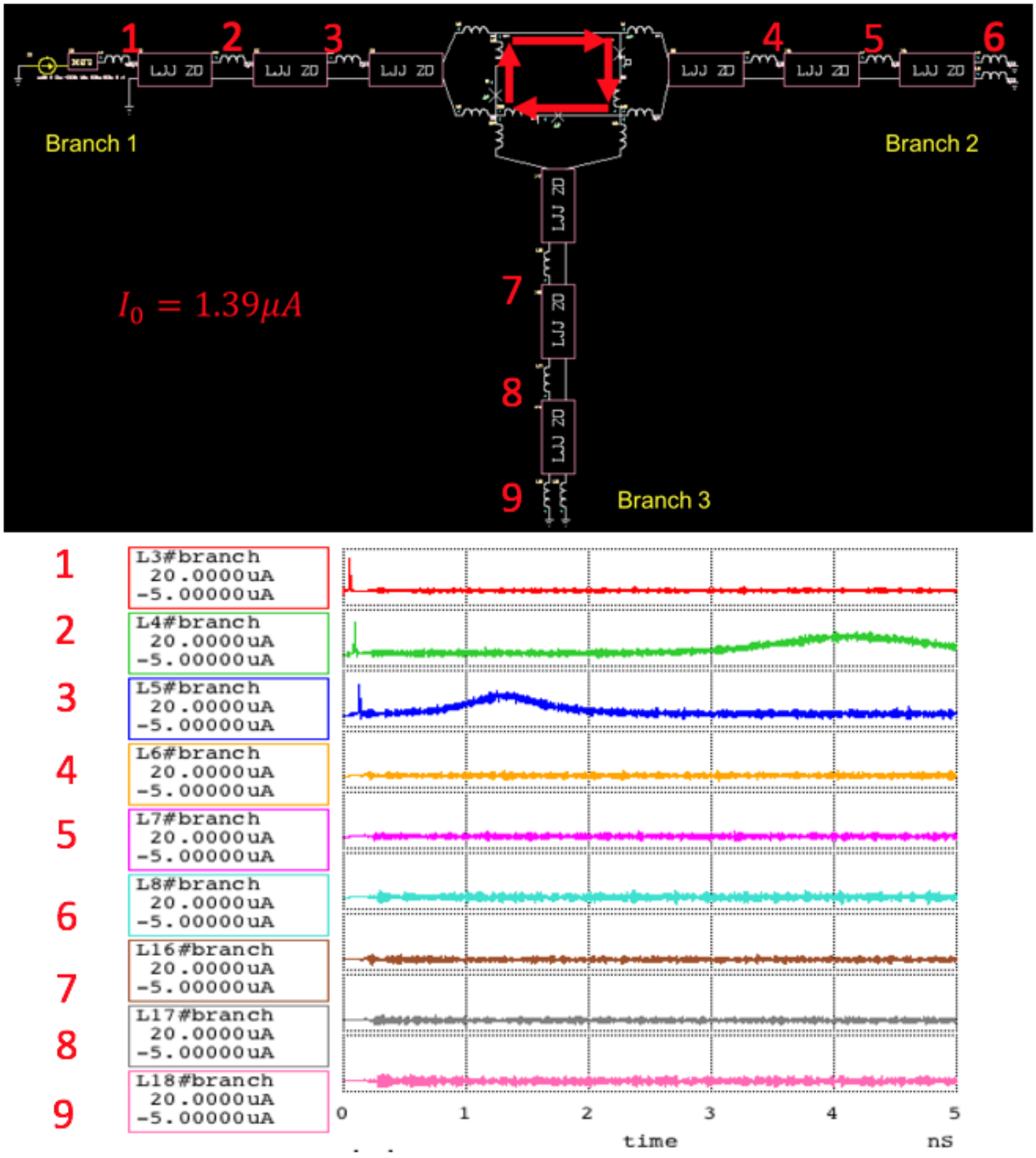

Figure B.4. Initial clockwise current of $I_0 = 1.39\mu A$

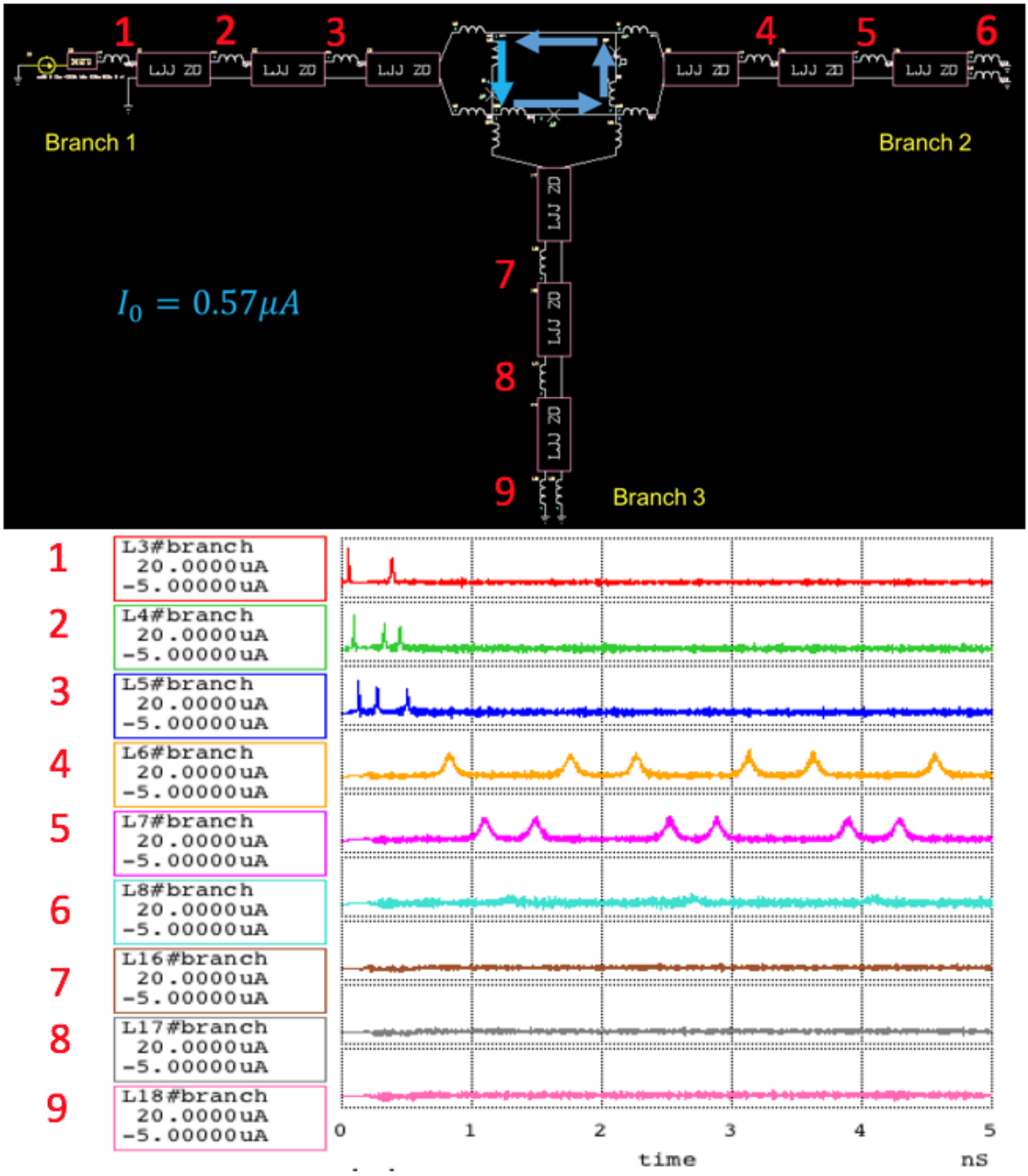

Figure B.5. Initial counter-clockwise current of $I_0 = 0.57\mu A$

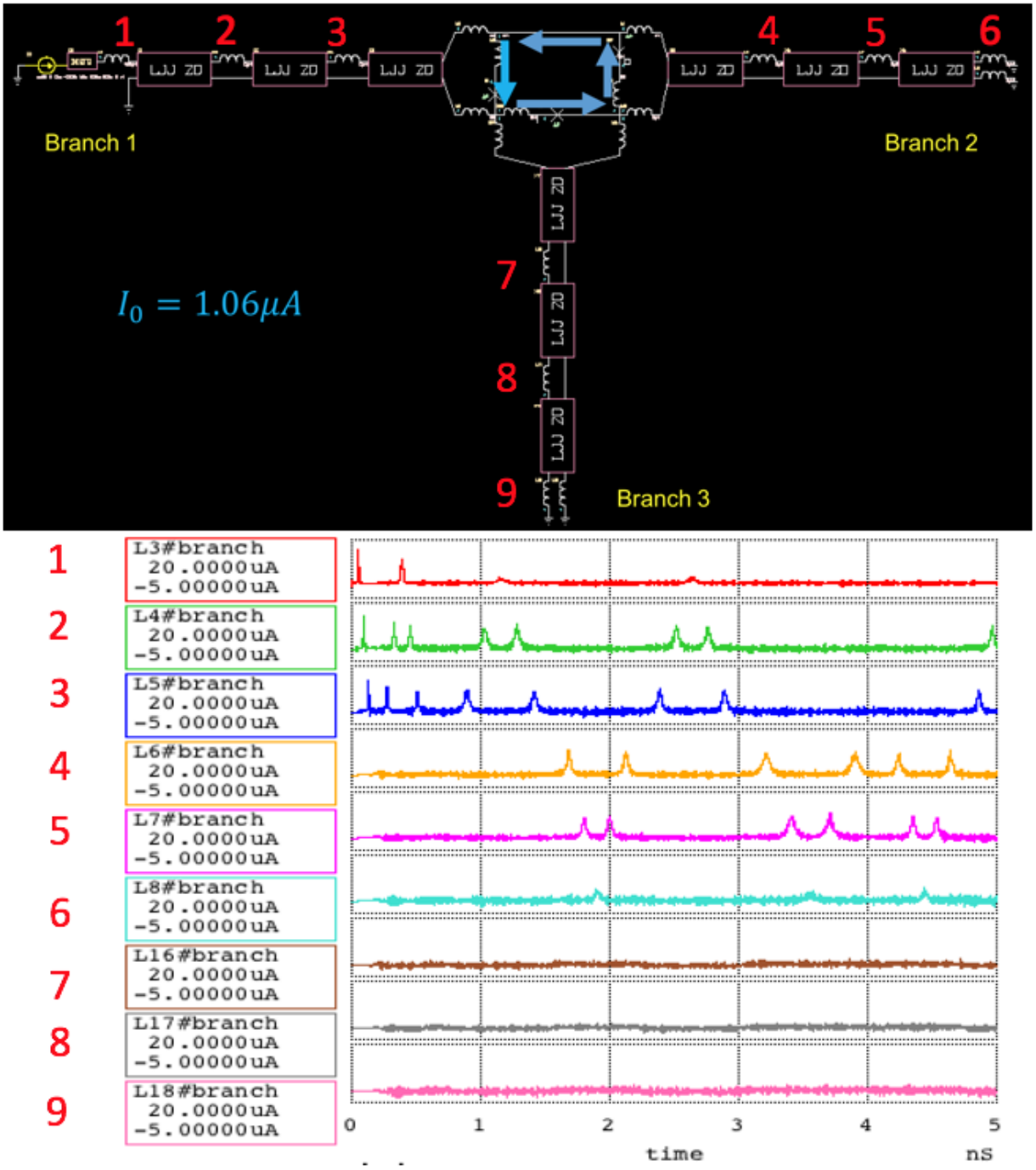

Figure B.6. Initial counter-clockwise current of $I_0 = 1.06\mu A$

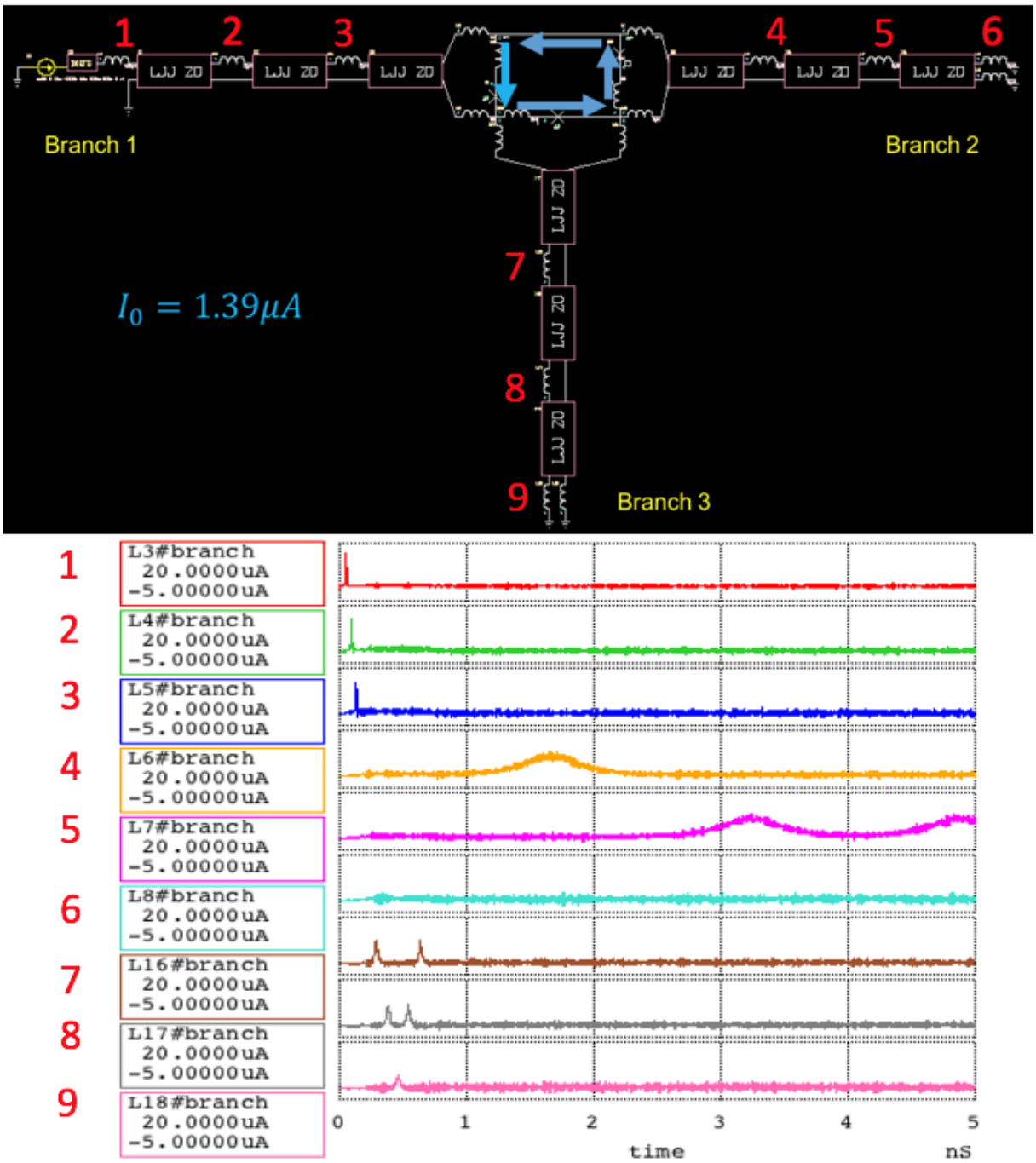

Figure B.7. Initial counter-clockwise current of $I_0 = 1.39\mu A$

C. APPENDIX: JJ ROTARY - BRANCHES 2 AND 3 SHORTED

In this appendix, we show simulation results for rotary branches terminals 2 and 3 shorted - the upper and lower inductors are connected with a wire. These results are shown in Figures C.1-C.3.

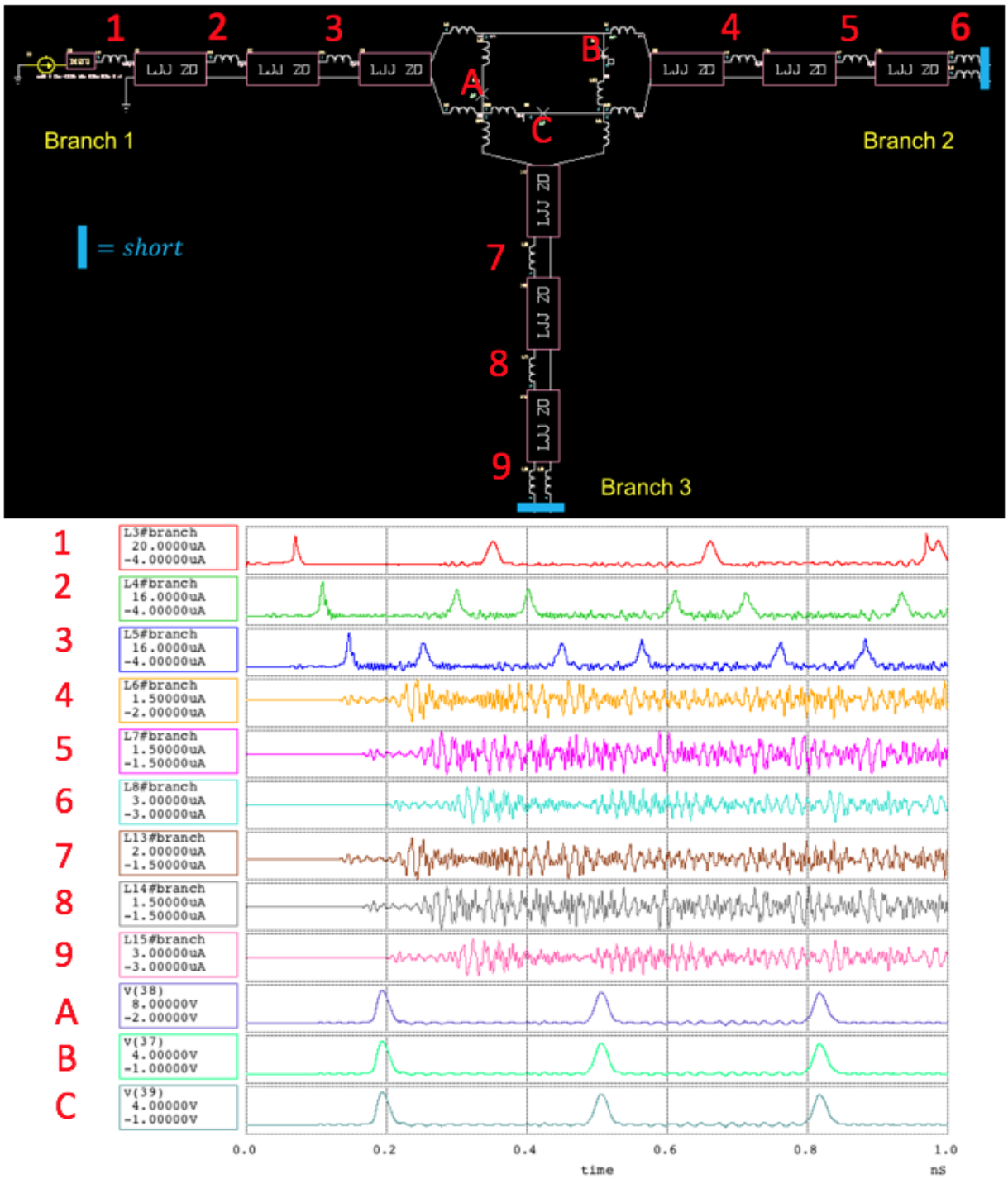

Figure C.1. Both branches 2 and 3 are terminated with a short.

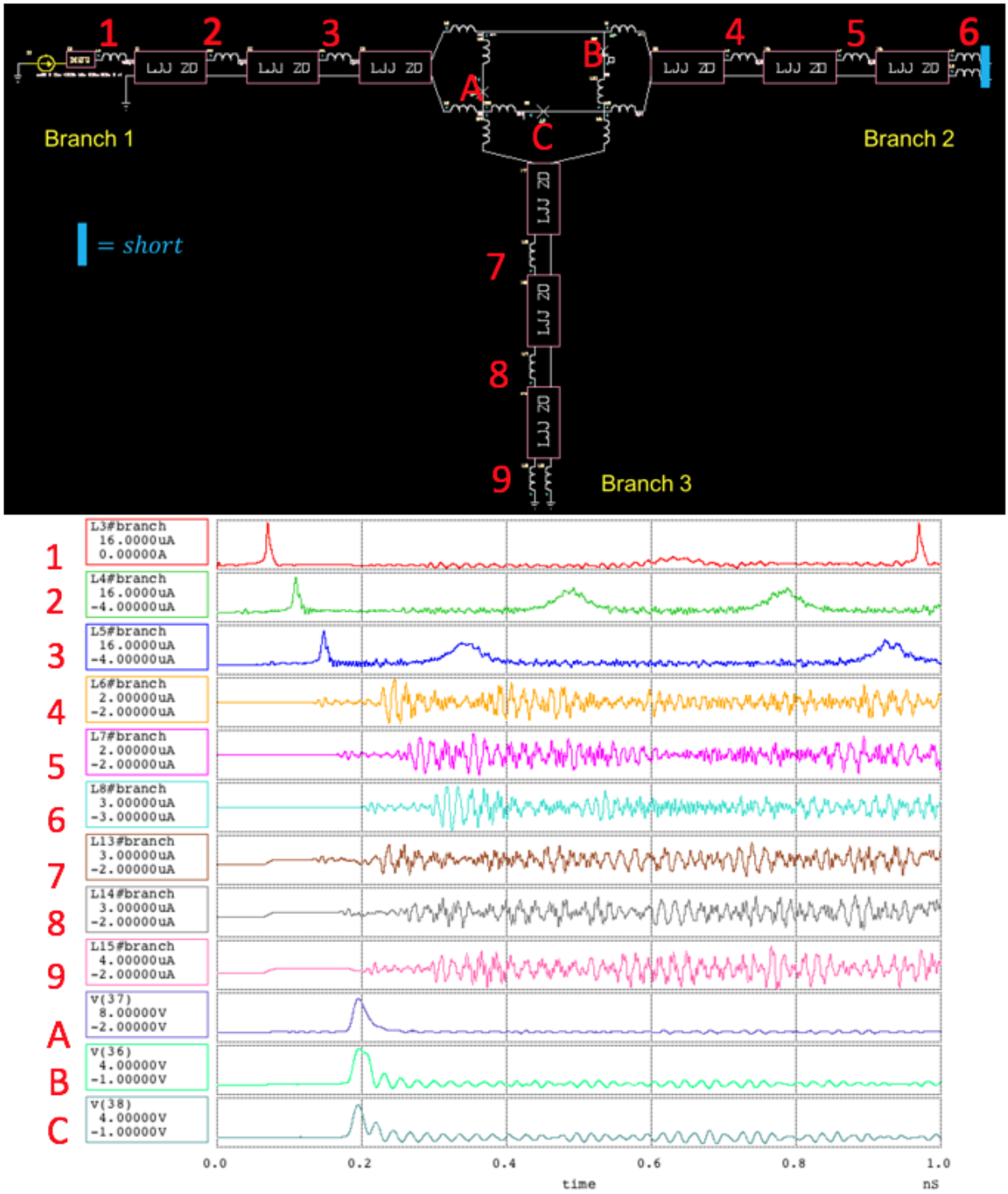

Figure C.2. Branches 2 is terminated with a short.

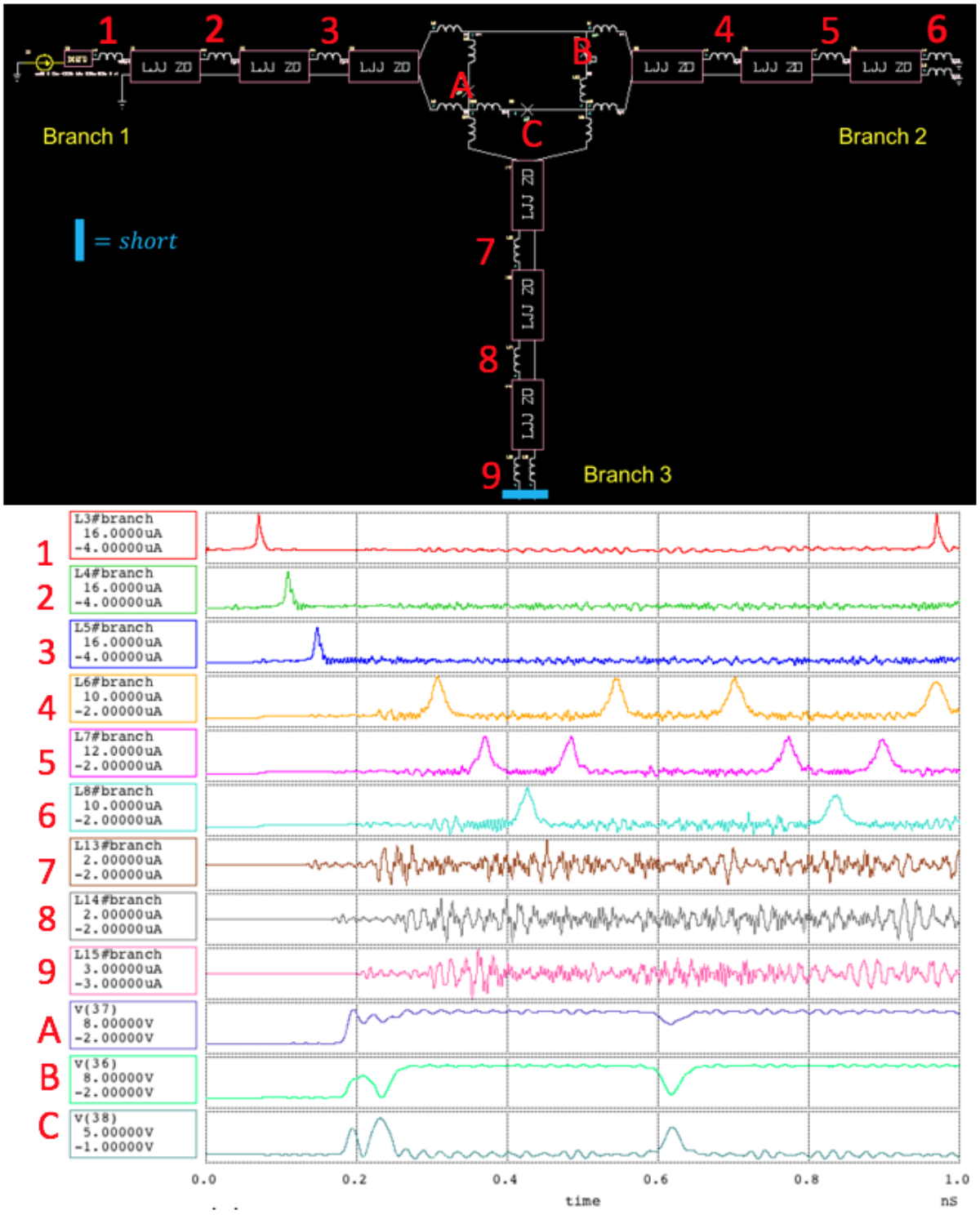

Figure C.3. Branch 3 is terminated with a short.

D. APPENDIX: MATHEMATICA CODES

In this appendix, we provide mathematica codes used for WRspice data extraction and fluxon visualization.

D.1 WRspice Data Extraction Code

WRspice was used to numerically simulate fluxon behavior (currents and JJ phases at different points in our circuit designs) and the code below was used to extract the data, obtain the raw data, group data type, and plot the parameter sweeps on either resistance values or initialized rotary currents. Each value corresponds to a different color on the plotted data. Below is the mathematica code used for this data extraction as seen in Figures D.1-D.3.

```
In[124]:= rawdata = Import[NotebookDirectory[] <> "res_sweep_1_16_5.txt", "Table"];
          sweepConditions = (*{}*)"R = " <> ToString[#] & /@ Range[1, 16, 5];
```

Figure D.1. Code for importing the sweep data (parameter sweep on either resistance or initialized current)

```
In[126]:= varLine = FirstPosition[rawdata, {"Variables:"}, 1][[1]]
          valLine = FirstPosition[rawdata, {"Values:"}, 1][[1]]

Out[126]= 9

Out[127]= 23

In[128]:= varNames = rawdata[[varLine + 1 ;; valLine - 1]][[ ;; , 2]]
          varUnits = rawdata[[varLine + 1 ;; valLine - 1]][[ ;; , 3]]

Out[128]= {time, L2#branch, L3#branch, L4#branch, L9#branch, L10#branch,
           L11#branch, L13#branch, L14#branch, L15#branch, v(39), v(40), v(41)}

Out[129]= {S, A, A, A, A, A, A, A, A, A, V, V, V}

In[130]:= varLabel = varNames[[#]] <> " (" <> varUnits[[#]] <> ")" & /@ Range[Length@varNames]

Out[130]= {time (S), L2#branch (A), L3#branch (A), L4#branch (A), L9#branch (A), L10#branch (A),
           L11#branch (A), L13#branch (A), L14#branch (A), L15#branch (A), v(39) (V), v(40) (V), v(41) (V)}
```

Figure D.2. Code for sweep data separation

```
In[131]:= curatedData =
    ({rawdata[[valLine + 1 ;; ;; Length[varNames]]][[ ;; , 2]]} ~ Join ~
       ParallelTable[rawdata[[valLine + 1 + vars ;; ;; Length[varNames]]][[ ;; , 1]],
        {vars, Length@varNames - 1}])ᵀ;

In[132]:= makeColorSegmentList[total_] := ColorData["DarkRainbow"][#] & /@ Subdivide[total - 1]
    numRuns = 4; lenSegment = Length[curatedData] / numRuns;
    If[IntegerQ[lenSegment], curatedDataSegmented = Partition[curatedData, lenSegment];
      colorSegmentList = makeColorSegmentList[numRuns];, Print["Could not segment data."];
      curatedDataSegmented = curatedData;
      Clear[colorSegmentList];];
    (*Length/@curatedDataSegmented*)

In[135]:= Clear[plotVar]
    plotVar[varnum_ ? (MemberQ[Range[Length[varNames]], #] &)] :=
     ListPlot[curatedData[[ ;; , {1, varnum}]], AxesLabel → {varLabel[[1]], varLabel[[varnum]]}]

In[137]:= Clear[plotVarSegmented]
    plotVarSegmented[varnum_ ? (MemberQ[Range[Length[varNames]], #] &)] :=
     ListLinePlot[curatedDataSegmented[[ ;; , ;; , {1, varnum}]], AxesLabel → {varLabel[[1]], varLabel[[varnum]]},
      PlotStyle → colorSegmentList, ImageSize → 400, FrameStyle → Gray,
      PlotLegends → Placed[sweepConditions, Above], PlotRange → Full]

▼In[139]:= GraphicsColumn[plotVarSegmented /@ Range[2, Length[varNames]], Spacings → Scaled[0.3], ImageSize → 500]
```

Figure D.3. Code for color-coding sweep data for value of resistance or initial current

D.2 Fluxon Visualization

Upon obtaining the raw data from our data extraction from WRspice, these data files were then used to create visualizations for fluxon propagation through the associated circuit designs. The code consists of data import, data normalization, image import of circuit design, image import, a scheme to locate sections on the image file to represent fluxon propagation (via change in red opacity) and JJ phase (via yellow rotating arrows), and video file generation. Below is the mathematica code for this task as can be seen in Figures D.4-D.12.

Importing data from WRspice

```
In[66]:= branch1one = Import[NotebookDirectory[] <> "branch1one_def", "Data"][[12 ;; All]];
In[67]:= branch1two = Import[NotebookDirectory[] <> "branch1two_def", "Data"][[12 ;; All]];
In[68]:= branch1three = Import[NotebookDirectory[] <> "branch1three_def", "Data"][[12 ;; All]];
In[69]:= branch2one = Import[NotebookDirectory[] <> "branch2one_def", "Data"][[12 ;; All]];
In[70]:= branch2two = Import[NotebookDirectory[] <> "branch2two_def", "Data"][[12 ;; All]];
In[71]:= branch2three = Import[NotebookDirectory[] <> "branch2three_def", "Data"][[12 ;; All]];
In[72]:= branch3one = Import[NotebookDirectory[] <> "branch3one_def", "Data"][[12 ;; All]];
In[73]:= branch3two = Import[NotebookDirectory[] <> "branch3two_def", "Data"][[12 ;; All]];
In[74]:= branch3three = Import[NotebookDirectory[] <> "branch3three_def", "Data"][[12 ;; All]];
```

Figure D.4. Code for importing the WRspice data for each of the currents at the 9 locations along the JJ rotary where the fluxon propagates.

Data with Normalized Currents

```
In[75]:= branch1one1 = ParallelTable[{branch1one[[2 count - 1, 2]], branch1one[[2 count, 2]]},
           {count, Length[branch1one] / 2}];
         maxbranch1one = Max[Table[branch1one1[[i]][[2]], {i, 1, Length[branch1one1]}]]
         normbranch1one =
           ParallelTable[{branch1one[[2 count - 1, 2]], branch1one[[2 count, 2]] / maxbranch1one},
           {count, Length[branch1one] / 2}];
         maxnormbranch1one = Max[Table[normbranch1one[[i]][[2]], {i, 1, Length[branch1one1]}]]
Out[76]= 0.0000155971
Out[78]= 1.
```

Figure D.5. Code for normalization of the data imported. This is done for all 9 locations along the JJ rotary.

Importing Phase Data

```
In[112]:= branch1phase = Import[NotebookDirectory[] <> "branch1phase_def", "Data"][[12 ;; All]];
In[113]:= branch2phase = Import[NotebookDirectory[] <> "branch2phase_def", "Data"][[12 ;; All]];
In[114]:= branch3phase = Import[NotebookDirectory[] <> "branch3phase_def", "Data"][[12 ;; All]];
```

Figure D.6. Code for importing of WRspice data for the phase on each of the 3 Josephson junctions.

Phase Data

```
In[115]:= branch1phase1 = ParallelTable[{branch1phase[[2 count - 1, 2]], branch1phase[[2 count, 2]]},
    {count, Length[branch1phase] / 2}];

In[116]:= branch2phase1 = ParallelTable[{branch2phase[[2 count - 1, 2]], branch2phase[[2 count, 2]]},
    {count, Length[branch2phase] / 2}];

In[117]:= branch3phase1 = ParallelTable[{branch3phase[[2 count - 1, 2]], branch3phase[[2 count, 2]]},
    {count, Length[branch3phase] / 2}];
```

Figure D.7. Code for separation of phase data.

Image

```
In[3]:= Import[
    "/Users/DewanWoods/Documents/Purdue University Files/Research/Superconductivity
      and Solitons/Mathematica
      Codes/wrspice-sweep-example/JJRotary_more_LJJs/JJRotaryMoreLJJs.png"]

In[118]:= rotaryimage =
```

```
;

In[119]:= {mywidth, myheight} = ImageDimensions[rotaryimage]

Out[119]= {1650, 846}
```

Figure D.8. Code for importing the JJ rotary image file.

```
In[60]:= Manipulate[Show[{rotaryimage, Graphics[{Red, Opacity[1], Disk[{mywidth relx, myheight rely}, mywidth 0.02]}]},
    ImageSize → 600], {relx, 0, 1}, {rely, 0, 1}]
```

Out[60]=

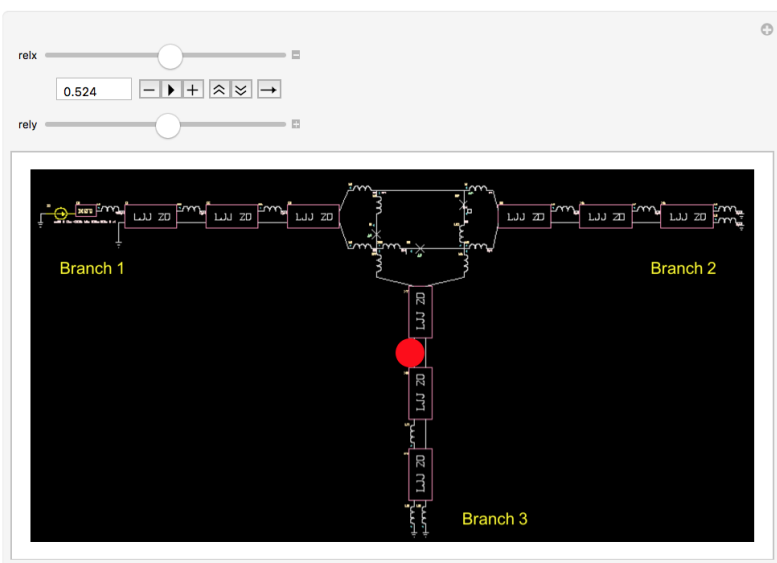

Figure D.9. Code showing a scheme for finding the location on the imported image for which the fluxon will propagate.

```
In[121]:= Manipulate[
  Show[
   {rotaryimage, Graphics[{Red, Opacity[Abs[normbranch1one[[Ceiling[time / timestep]]][[2]]]],
      Disk[{mywidth .13, myheight .89}, mywidth 0.02], Red, Opacity[Abs[normbranch1two[[Ceiling[time / timestep]]][[2]]]],
      Disk[{mywidth .22, myheight .89}, mywidth 0.02], Red,
      Opacity[Abs[normbranch1three[[Ceiling[time / timestep]]][[2]]]], Disk[{mywidth .34, myheight .89}, mywidth 0.02],
      Red, Opacity[Abs[normbranch2one[[Ceiling[time / timestep]]][[2]]]], Disk[{mywidth .74, myheight .89}, mywidth 0.02],
      Red, Opacity[Abs[normbranch2two[[Ceiling[time / timestep]]][[2]]]], Disk[{mywidth .85, myheight .89}, mywidth 0.02],
      Red, Opacity[Abs[normbranch2three[[Ceiling[time / timestep]]][[2]]]],
      Disk[{mywidth .96, myheight .89}, mywidth 0.02], Red, Opacity[Abs[normbranch3one[[Ceiling[time / timestep]]][[2]]]],
      Disk[{mywidth .528, myheight .5}, mywidth 0.02], Red, Opacity[Abs[normbranch3two[[Ceiling[time / timestep]]][[2]]]],
      Disk[{mywidth .528, myheight .29}, mywidth 0.02], Red,
      Opacity[Abs[normbranch3three[[Ceiling[time / timestep]]][[2]]]], Disk[{mywidth .528, myheight .08}, mywidth 0.02],
      Yellow, Opacity[1], Arrowheads[.03], Rotate[Arrow[{{mywidth .48, myheight .85}, {mywidth .48, myheight .86}}],
       branch1phase1[[Ceiling[time / timestep]]][[2]], {mywidth .48, myheight .830}], Yellow, Arrowheads[.03],
      Rotate[Arrow[{{mywidth .6, myheight .92}, {mywidth .6, myheight .93}}],
       branch2phase1[[Ceiling[time / timestep]]][[2]], {mywidth .6, myheight .90}], Yellow, Arrowheads[.03],
      Rotate[Arrow[{{mywidth .54, myheight .81}, {mywidth .54, myheight .82}}],
       branch3phase1[[Ceiling[time / timestep]]][[2]], {mywidth .54, myheight .79}]}]}, ImageSize → 400],
  {time, timestep / 100, 1}]
```

Out[121]=

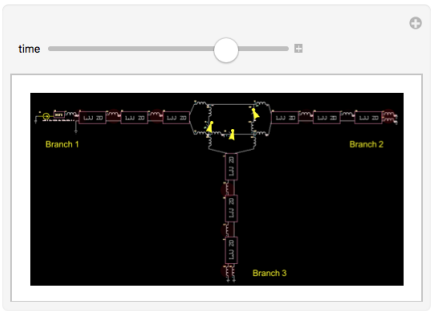

Figure D.10. A test showing the complete visualization before generating video file.

Generating Video File

```
In[122]:= rotaryLJJstable3jj =
  Table[
   Show[
    {rotaryimage, Graphics[{Red, Opacity[Abs[normbranch1one[[100 count]][[2]]]],
       Disk[{mywidth .11, myheight .896}, mywidth 0.02], Red, Opacity[Abs[normbranch1two[[100 count]][[2]]]],
       Disk[{mywidth .22, myheight .896}, mywidth 0.02], Red, Opacity[Abs[normbranch1three[[100 count]][[2]]]],
       Disk[{mywidth .33, myheight .896}, mywidth 0.02], Red, Opacity[Abs[normbranch2one[[100 count]][[2]]]],
       Disk[{mywidth .74, myheight .896}, mywidth 0.02], Red, Opacity[Abs[normbranch2two[[100 count]][[2]]]],
       Disk[{mywidth .85, myheight .896}, mywidth 0.02], Red, Opacity[Abs[normbranch2three[[100 count]][[2]]]],
       Disk[{mywidth .96, myheight .896}, mywidth 0.02], Red, Opacity[Abs[normbranch3one[[100 count]][[2]]]],
       Disk[{mywidth .526, myheight .51}, mywidth 0.02], Red, Opacity[Abs[normbranch3two[[100 count]][[2]]]],
       Disk[{mywidth .526, myheight .29}, mywidth 0.02], Red, Opacity[Abs[normbranch3three[[100 count]][[2]]]],
       Disk[{mywidth .526, myheight .08}, mywidth 0.02], Yellow, Opacity[1], Arrowheads[.03],
       Rotate[Arrow[{{mywidth .48, myheight .85}, {mywidth .48, myheight .86}}], branch1phase1[[100 count]][[2]],
        {mywidth .48, myheight .830}], Yellow, Arrowheads[.03],
       Rotate[Arrow[{{mywidth .6, myheight .92}, {mywidth .6, myheight .93}}], branch2phase1[[100 count]][[2]],
        {mywidth .6, myheight .90}], Yellow, Arrowheads[.03],
       Rotate[Arrow[{{mywidth .54, myheight .81}, {mywidth .54, myheight .82}}], branch3phase1[[100 count]][[2]],
        {mywidth .54, myheight .79}]}]}, ImageSize → 600], {count, Length[normbranch3three] / 100}];
```

Figure D.11. Code for generation of video file

```
In[123]:= Export[NotebookDirectory[] <> "3JJrotary_def(3).mov", rotaryLJJstable3jj, "QuickTime", "FrameRate" → 20]

Out[123]= /Users/DewanWoods/Documents/Purdue University Files/Research/Superconductivity
  and Solitons/Mathematica Codes/wrspice-sweep-example/JJRotary_more_LJJs/3JJrotary_def(3).mov
```

Figure D.12. Code for generating video file for a given file name